Constraining the geothermal parameters of *in situ* Rb–Sr dating on Proterozoic shales and their subsequent applications

Darwinaji Subarkah[1,6], Angus L. Nixon[2,6], Monica Jimenez[3], Alan S. Collins[1,6], Morgan L. Blades[1], Juraj Farkaš[4,6], Sarah E. Gilbert[5], Simon Holford[3], and Amber Jarrett[7]

[1]Tectonics & Earth Systems (TES), Department of Earth Sciences, University of Adelaide, Adelaide, SA 5005, Australia
[2]Apatite Thermochronology Lab and Services (ATLaS), Department of Earth Sciences, University of Adelaide, Adelaide, SA 5005, Australia
[3]Stress, Structure and Seismic, Australian School of Petroleum and Energy Resources (ASPER), University of Adelaide, Adelaide, SA 5005, Australia
[4]Metal Isotope Group (MIG), Department of Earth Sciences, University of Adelaide, Adelaide, SA 5005, Australia
[5]Adelaide Microscopy, University of Adelaide, Adelaide, SA 5005, Australia
[6]MinEx CRC, Australian Resources Research Centre, Perth, WA 6151, Australia
[7]Northern Territory Geological Survey, Darwin, NT 0801, Australia

Correspondence to: Darwinaji Subarkah (Darwinaji.subarkah@adelaide.edu.au)

Abstract Recent developments in tandem laser ablation-mass spectrometer technology have demonstrated capacity for separating parent and daughter isotopes of the same mass online. As a result, beta decay chronometers can now be applied to the geological archive *in situ* as opposed to through traditional whole-rock digestions. One novel application of this technique is the *in situ* Rb–Sr dating of Proterozoic shales that are dominated by authigenic clays such as illite. This method can provide a depositional window for shales by differentiating signatures of early diagenetic processes versus late-stage secondary alteration. However, the hydrothermal sensitivity of the Rb–Sr isotopic system across geological timescales in shale-hosted clay minerals is not well understood. As such, we dated the Mesoproterozoic Velkerri Formation from the Altree 2 well in the Beetaloo Sub-basin (greater McArthur Basin), northern Australia, using this approach. We then constrained thermal history of these units using common hydrocarbon maturity indicators, and modelled effects of contact heating due to the intrusion of the Derim Derim Dolerite.

In situ Rb–Sr dating of mature, oil-prone shales in the diagenetic zone from the Velkerri Formation yielded ages of 1448 ± 81 Ma, 1434 ± 19 Ma, and 1421 ± 139 Ma. These results agree with previous Re–Os dating of the unit and are interpreted as recording the timing of an early diagenetic event soon after deposition. Conversely, overmature, gas-prone shales in the anchizone sourced from deeper within the borehole were dated at 1322 ± 93 Ma and 1336 ± 40 Ma. These ages are younger than the expected depositional window for the Velkerri Formation. Instead, they are consistent with the age of the Derim Derim Dolerite mafic intrusion intersected 800 m below the Velkerri Formation. Thermal modelling suggests that a single intrusion of 75 m thickness would have been capable of

producing a significant hydrothermal perturbation radiating from the sill top. The intrusion width proposed by this model is consistent with similar Derim Derim Dolerite sill thicknesses found elsewhere in the McArthur Basin. The extent of the hydrothermal aureole induced by this intrusion coincide with the window in which kerogen from the Velkerri Formation becomes overmature. As a result, the mafic intrusion intersected here is interpreted to have caused kerogen in these shales to enter the gas window, induced fluids that mobilise trace elements and reset the Rb–Sr chronometer. Consequently, we propose that the Rb–Sr chronometer in shales may be sensitive to temperatures of ca. 120°C in hydrothermal reactions but can withstand temperatures of more than 190°C in thermal systems not dominated by fluids. Importantly, this study demonstrates a framework for the combined use of *in situ* Rb–Sr dating and kerogen maturation indicators to help reveal the thermochronological history of Proterozoic sedimentary basins. As such, this approach can be a powerful tool for identifying the hydrocarbon potential of source rocks in similar geological settings.

1 Introduction

The Rb–Sr isotopic system has historically been one of the most powerful dating tools in Earth science. Rb is abundant in K-rich minerals such as micas, clays, and K-feldspar, and these minerals are commonly found in a wide range of geological settings (Simmons, 1998). Therefore it is an effective technique to date processes such as igneous emplacement, metamorphism, sedimentation, clay authigenesis, and hydrothermal alteration when these phases can be differentiated (Nebel, 2014). Its long half-life also makes it applicable to date events as early as the infant stages of our solar system (Minster et al., 1979; Nebel et al., 2011; Papanastassiou and Wasserburg, 1970). Traditionally, the application of this method required an arduous process of column chromatography to chemically separate the parent (^{87}Rb) and daughter (^{87}Sr) isotopes and avoid isobaric interference between the two elements (Charlier et al., 2006; Dickin, 2018; Faure, 1977; Hahn et al., 1943; Hahn and Walling, 1938; Yang et al., 2010). Alas, this approach has historically been expensive, time consuming, and results in the loss of the genetic relationships between the minerals analysed, causing the technique to lose its popularity in recent years (Nebel, 2014).

Recent advancements in tandem laser ablation inductively coupled plasma mass spectrometry (LA-ICP-MS/MS) and similar instruments have revitalised the use of Rb–Sr by allowing them to be applied *in situ* (Bevan et al., 2021b; Gorojovsky and Alard, 2020; Hogmalm et al., 2017; Redaa et al., 2021a; Yim et al., 2021; Zack and

Hogmalm, 2016). Reactive gasses such as N_2O and SF_6 can be introduced into a reaction cell between quadrupoles in an LA-ICP-MS/MS system, which permits the online separation of ^{87}Sr from ^{87}Rb through the measurement of the mass shifted Sr reaction product (Hogmalm et al., 2017; Redaa et al., 2021a; Zack and Hogmalm, 2016). This allows for a more rapid and economic analysis time, as well as the ability to preserve petrographic relationships during these analyses. Consequently, secondary input of Rb or Sr from inclusions, zonation, alteration, and detritus can be isolated, resulting in a better understanding of the geochronological results. However, it should be noted that nm or μm sized mineral intergrowths of different origins still provide challenges when large spot sizes are used. The application of similar setups with other beta-decay dating systems have also yielded promising results (Bevan et al., 2021a; Brown et al., 2022; Gorojovsky and Alard, 2020b; Harrison et al., 2010; Hogmalm et al., 2019; Ribeiro et al., 2021; Rösel and Zack, 2022; Scheiblhofer et al., 2022; Simpson et al., 2021; Simpson et al., 2022; Tamblyn et al., 2021).

Hence, the *in situ* Rb–Sr dating method can now be used very similarly to laser ablation U–Pb dating, where age information can be obtained reliably, rapidly, and cheaply. In addition, the initial $^{87}Sr/^{86}Sr$ ratio from the calculated isochron and the elemental data concurrently collected with the Rb and Sr isotopes can fingerprint the geochemical nature of the samples analysed (Li et al., 2020; Redaa et al., 2021b; Subarkah et al., 2021; Tamblyn et al., 2020). This approach has been shown to be capable of dating paragenetic sequences in deformation structures (Armistead et al., 2020; Tillberg et al., 2020), hydrothermal alteration assemblages (Laureijs et al., 2021a; Laureijs et al., 2021b), magmatic and metamorphic events (Li et al., 2020; Tamblyn et al., 2020), as well as metallogenic systems (Olierook et al., 2020; Redaa et al., 2021b; Şengün et al., 2019) whilst still preserving their micro-scale textural context.

Another novel use of this technique is to date Proterozoic shales in order to constrain their depositional window (Subarkah et al., 2021). Evidence suggests that clay minerals in Proterozoic shales are dominated by authigenic products from reverse weathering processes during reactions in equilibrium with the formation waters (Deepak et al., 2022; Isson and Planavsky, 2018; Kennedy et al., 2006; Mackenzie and Kump, 1995; Rafiei and Kennedy, 2019; Rafiei et al., 2020). Conversely, clay assemblages in late Ediacaran and Phanerozoic shales are commonly dominated by detrital products from continental weathering and erosion of soils and unstable parent rocks (Baldermann et al., 2020; Chamley, 1989; Galán, 2006; Hillier, 1995; Kennedy et al., 2006; Rafiei et al., 2020;

Singer, 1980; Wilson, 1999). Simple multicellular organisms such as fungi and lichen have been shown to dramatically influence the rate of chemical weathering in continental rocks (Chen et al., 2000; Cuadros, 2017; Kennedy et al., 2006; Lee and Parsons, 1999; McMahon and Davies, 2018; Mergelov et al., 2018; Rafiei et al., 2020). As such, the surge in abundance of detrital clays in shales in the Ediacaran and Phanerozoic has been attributed to the production of soils driven by emergence of these microorganisms (Kennedy et al., 2006; Lee and Parsons, 1999; McMahon and Davies, 2018; Mergelov et al., 2018; Rafiei and Kennedy, 2019; Zambell et al., 2012). Thus, the primarily authigenic nature of clay minerals in Proterozoic shales make them ideal targets for *in situ* Rb–Sr dating (Subarkah et al., 2021).

Despite the promising potential of the Rb–Sr isotopic system, the chronometer still holds some limitations. Rb and Sr are large ion lithophile elements that can sit in well-bound interstitial sites within a mineral lattice as well as adsorbed onto the surface where they are more susceptible to fluid mobilisation (Li et al., 2019; Nebel, 2014; Villa, 1998). In these environments, fluid-induced recrystallisation and alteration can drive element and isotopic exchange at lower effective closure temperatures than those empirically determined for classic thermal volume diffusion reactions (Dodson, 1973; Field and Råheim, 1979; Jenkin et al., 1995; Villa, 1998). Nevertheless, these complications can in turn be used advantageously to date secondary events such as episodes of hydrothermal fluid-flow (Dodson, 1973; Li et al., 2020; Redaa et al., 2021b; Shepherd and Darbyshire, 1981; Subarkah et al., 2021; Tamblyn et al., 2020). However, it should be noted that the Rb–Sr system in shale-hosted illite may also be affected during diagenesis via the transformation of smectite to illite-smectite mixed layer minerals.

In this study, we dated the Mesoproterozoic Velkerri Formation from the Roper Group of the McArthur Basin in northern Australia by *in situ* Rb–Sr geochronology and show that clay-mineral recrystallization in these shales occur at similar temperatures to kerogen catagenesis. The Roper Group is a good case study for *in situ* Rb–Sr shale dating, as it has been shown to be dominated by authigenic clays (Rafiei and Kennedy, 2019; Subarkah et al., 2021) and is chronologically well-constrained (Ahmad and Munson, 2013; Bodorkos et al., 2022; Cox et al., 2022; Kendall et al., 2009; Southgate et al., 2000; Subarkah et al., 2021; Yang et al., 2020). Furthermore, the resurgence of interest in the resource potential of the organic-rich Velkerri Formation has also yielded a framework of palaeotemperature data that aim to discern the maturation history of hydrocarbons within the unit (Ahmad and Munson, 2013; Capogreco,

2017; Cox et al., 2016; Crick et al., 1988; George and Ahmed, 2002a; Jarrett et al., 2019a; Lemiux, 2011; Revie, 2014; Summons et al., 1994; Taylor et al., 1994; Volk et al., 2005).

Here, we targeted the Velkerri Formation (Figure 1) from the thoroughly investigated well Altree 2 (Capogreco, 2017; Cox et al., 2022; Cox et al., 2016; George and Ahmed, 2002a; Jarrett et al., 2019a; Lemiux, 2011; Nguyen et al., 2019; Nixon et al., 2021; NTGS, 1989, 2009, 2010, 2012; Revie, 2014; Sander et al., 2018; Yang et al., 2018). We show that common hydrocarbon maturation proxies such as T_{max} data from Rock-Eval pyrolysis, aromatic hydrocarbons, bitumen reflectance, and illite crystallinity can help define the temperature sensitivity of the Rb–Sr isotopic system in organic-rich shales. In addition, we have also modelled the geothermal aureole of a mafic intrusion that may have matured the kerogen into the gas window, altered trace elemental signatures and reset the Rb–Sr isotopic system within the unit. As a result, we demonstrate that combining this novel dating method with traditional kerogen maturation proxies can be a powerful tool for reconstructing the thermochronological evolution of Proterozoic basin systems. This approach can then be applied to aid in hydrocarbon exploration for similar settings.

2 Geological Background

The Palaeo-to-Mesoproterozoic greater McArthur Basin is an intra-cratonic sedimentary system exposed across 180,000 km^2 of northern Australia (Ahmad and Munson, 2013). The basin is sub-divided into five unconformity-bounded sedimentary packages characterized by similarities in age, lithology, and stratigraphic position (Jackson et al., 1999; Rawlings, 1999). The Roper Group is part of the Wilton Package which is the youngest of these sub-divisions (Jackson et al., 1999; Jackson et al., 1987; Munson, 2016; Rawlings, 1999). The thickness of the Roper Group varies around 1 to 5 km across several different fault zones (Abbott and Sweet, 2000; Abbott et al., 2001; Ahmad and Munson, 2013; Jackson et al., 1987; Rawlings, 1999). The Beetaloo Sub-basin (Figure 1) is interpreted to be the main depocentre of the sedimentary system and preserves the thickest Roper Group sequences (Abbott and Sweet, 2000; Ahmad and Munson, 2013; Jackson et al., 1987; Plumb and Wellman, 1987). Lithologically, the Roper Group comprises of a series of coarsening-up sequences dominated by marine mudstone and interbedded sandstone with minor successions of intraclastic limestone (Abbott and Sweet, 2000; Jackson et al., 1987; Munson, 2016; Yang et al., 2018). Records of water-column euxinia and redox stratification, as well as fluctuating salinity levels, suggests that the Roper Group formed in an intermittently restricted marine basin within an epicontinental setting

similar to the modern Black Sea, or Baltic Sea (Ahmad and Munson, 2013; Cox et al., 2022; Cox et al., 2016; Mukherjee and Large, 2016; Revie and MacDonald, 2017; Yang et al., 2018).

Age constraints of the Roper Group have been established through several geochronological methods (Ahmad and Munson, 2013; Jackson et al., 1999; Kendall et al., 2009; Nixon et al., 2021; Page et al., 2000; Southgate et al., 2000; Subarkah et al., 2021; Yang et al., 2019; Yang et al., 2020; Yang et al., 2018). The beginning of the group's genesis is bracketed by a SHRIMP U–Pb zircon study from a tuff within the unconformably underlying Nathan Group as well as minimum depositional age from an *in situ* Rb–Sr analysis in the lower Roper Group that yielded ages of 1589 ± 3 Ma and 1577 ± 56 Ma, respectively (Page et al., 2000; Subarkah et al., 2021). The unconformity between the Roper Group and the immediately underlying Nathan Group is likely related to the Isan Orogeny ca. 1.58 Ga (Ahmad and Munson, 2013; Jackson et al., 1999). Absolute dating of the Roper Group has been obtained through two SHRIMP U–Pb zircon studies from tuff layers in the Mainoru Formation resulting in ages of 1492 ± 4 Ma and 1493 ± 4 Ma (Jackson et al., 1999; Southgate et al., 2000). On the other hand, the Kyalla Formation at the top of the Roper Group is constrained to being deposited between the U–Pb age of its youngest detrital zircon at 1313 ± 47 Ma (Yang et al., 2018) and the age of crosscutting Derim Derim dolerite intrusions at 1313 ± 1 Ma, 1324 ± 4 Ma, and 1327.5 ± 0.6 Ma (Bodorkos et al., 2022; Yang et al., 2020).

Mature organic-rich shales from the Velkerri Formation have been dated by Re–Os analysis at 1417 ± 29 Ma and 1361 ± 21 Ma (Kendall et al., 2009). These ages have been interpreted to be the depositional age of the formation. The geochronological constraints of the Roper Group are summarized in Figure 1. The Velkerri Formation is dominated by deep-basinal lithologies such as mudstones and siltsones that coarsens-up into the cross-bedded Moroak Sandstone and Sherwin Ironstone (Abbott et al., 2001). The Velkerri Formation is interpreted to represent a deep-water, high-stand systems tract within a marine environment (Abbott et al., 2001; Warren et al., 1998). The Velkerri Formation is commonly sub-divided into three distinct members (from bottom to top, the Kalala, Amungee, and Wyworrie Members) based on variations in total organic carbon (TOC) content, gamma ray response, geochemistry, sedimentology and mineralogy (Ahmad and Munson, 2013; Cox et al., 2016; Cox et al., 2019; Jarrett et al., 2019b; Munson and Revie, 2018; Revie, 2016; Warren et al., 1998).

Importantly, the McArthur Basin experienced a complex thermal history following the deposition of the Roper Group Mafic sills of the Derim Derim Dolerite widely intrude all units in the Roper Group at ca. 1330–1300 Ma,

with the oldest intrusions likely contemporaneous with the end of sedimentation in the basin (Ahmad and Munson, 2013; Bodorkos et al., 2022; Nixon et al., 2021; Subarkah et al., 2021; Yang et al., 2020). Little evidence of subsequent tectono-thermal perturbation is present within the basin until much of the region was overlain by subaerial basaltic lavas of the Kalkarindji Large Igneous Province (LIP) extruded at ca. 510 Ma (Evins et al., 2009; Glass and Phillips, 2006; Jourdan et al., 2014; Nixon et al., 2022). Following the Cambrian eruption of the Kalkarindji lavas, no significant (> 110°C) heating has been detected within the shallow parts of the basin (Duddy et al., 2004; Nixon et al., 2022).

The Altree 2 well drilled in the Beetaloo Sub-basin was chosen for this study as it intersects the entirety of the Velkerri Formation (Figure 2). In addition, the well also intersected lavas of the Kalkarindji LIP directly overlying the Proterozoic sedimentary rocks and terminated at an intrusion of the Derim Derim Dolerite. Importantly, this well has also been the focus of numerous geochronological, geochemical and geobiological investigations from academia, private explorers as well as the Northern Territory Geological Survey (NTGS) which provide important complementary data to supplement this study (Bodorkos et al., 2022; Cox et al., 2022; Cox et al., 2016; Cox et al., 2019; George and Ahmed, 2002a; Jarrett et al., 2019a; Lemiux, 2011; Nguyen et al., 2019; Nixon et al., 2021; NTGS, 2009, 2010, 2012; Sander et al., 2018; Warren et al., 1998; Yang et al., 2018).

3 Methodology

Rock-Eval pyrolysis, aromatic hydrocarbon results, bitumen reflectance values, bulk x-ray diffraction (XRD) mineralogical compositions, and well log data were collated from several sources and compiled together in this study (Capogreco, 2017; Cox et al., 2016; Jarrett et al., 2019b; Lemiux, 2011; NTGS, 1989, 2009, 2010, 2012; Revie, 2014; Revie et al., 2022). As such, their corresponding methodologies can be found in the references therein. The lithology of the Velkerri Formation was interpreted in detail (Figure 2) using the electrical logs Gamma-Ray (GR), Neutron (NRS) and Density (RHOB) of the Altree-2 well (NTGS, 1989). Four lithologies were defined after applying cut-offs at each electrical log. They are then correlated along depth. Sandstone units corresponds to a GR < 130 API, NRS < 0.20 % and RHOB of around 2.5 g/cm^3. This relates to a cross over between the RHOB and NPRS logs and competent material at the GR. Interbedded shale and sands are defined by a GR > 130 and < 250 API, NRS > 0.20 and < 0.25 m^3/m^3 and RHOB between 2.5 and 2.53 g/cm^3. This lithology reflected a smaller breach between the density and neutron logs in comparison to the previous sandstone lithology. Shale units were constrained by a

GR > 250 API, Neutron > 0.25 m^3/m^3 and RHOB > 2.53 g/cm^3 and a minimum to no separation between the porosity logs. On the other hand, dolomitic siltstones have a GR response similar to the sandstone, with NRS ranging between 0.25 to 0.27 and RHOB > 2.62 g/cm^3. This indicates a competent lithology in the GR with a gap between the neutron and density curves. In addition, T_{max} data werealso collated to discriminate the hydrocarbon maturation levels downhole. From this, a shift in hydrocarbon potential and T_{max} gradients were identified at around 900 m (Figure 2), where kerogen enters the gas window and becomes overmature. Five shale chips were then sampled from the Velkerri Formation in Altree 2 at depths of 415 m, 520 m, 696 m, 938 m, and 1220 m for further characterisation.

Samples were first imaged for their mineral composition and petrographic relationships. Back Scatter Electron (BSE) imaging and Mineral Liberation Analysis (MLA) maps of samples were collected using a Hitachi SU3800 Automated Mineralogy Scanning Electron Microscope at Adelaide Microscopy. BSE image tiles were done at 10 mm working distance and 20kV acceleration voltage with MLA maps were completed using a raster analysis with spectra collected at 0.35 µm/pixel resolution. Minerals previously categorised by bulk XRD analysis of the Velkerri Formation from Cox et al. (2016) were used to develop a 'library' to help identify phases found by spectral reflectance MLA mapping. *In situ* Rb–Sr geochronology and trace element analysis were undertaken at Adelaide Microscopy using a laser ablation (RESOlution-LR ArF 193nm excimer laser) inductively coupled plasma tandem mass spectrometer (Agilent 8900x ICP-MS/MS) with the analytical parameters and tuning conditions following Redaa et al. (2021a). The laser set-up used in this study is provided in the Supplementary Material. Laser ablation data and error correlations were processed using the LADR software package (Norris and Danyushevsky, 2018; Schmitz and Schoene, 2007). During the data-processing step, Zr, Si, Ti, and rare earth element signatures were monitored to filter the detrital component of each analysis. Non-stable isotopic and elemental signatures were also culled or cropped during the processing of each analysis to aid in ensuring spot homogeneity. The ^{87}Rb decay constant used was 0.000013972 ± 4.5e-7 Myr^{-1} following Villa et al. (2015). Isochron and single-spot ages were calculated with ISOPLOTR (Vermeesch, 2018). Single-spot ages were calculated using the isochron intercept as their initial $^{87}Sr/^{86}Sr$ ratios (Nebel, 2014; Rösel and Zack, 2022; Vermeesch, 2018). In addition, kernel density estimation (KDE) graphs (Vermeesch, 2012), cumulative age distributions (CAD) plots (Vermeesch, 2007), and multidimensional scaling (MDS) graphs (Vermeesch, 2013) were also constructed using ISOPLOTR (Vermeesch, 2018) to differentiate between the population of single-spot ages from each sample.

The phlogopite nano-powder Mica-Mg (Govindaraju et al., 1994) was used as the primary reference material and its natural mineral equivalent MDC from the Ampandrandava Mine in Madagascar (Armistead et al., 2020; Hogmalm et al., 2017; Li et al., 2020; Redaa et al., 2021a) as well as glauconite grain reference material GL-O (Charbit et al., 1998; Derkowski et al., 2009) were used secondary age standards. As previously discussed in Subarkah et al. (2021), nano-powdered reference materials have similar ablation characteristics to fine-grained shales, with analogous matrix effects. As such, they are ideal standards for *in situ* analyses of these samples.

When anchored to a $^{87}Sr/^{86}Sr$ initial ratio = 0.72607 ± 0.00363 as reported by Hogmalm et al. (2017), MDC yielded an age of 524 ± 7 Ma. This is within error of the published mean age of Mica-Mg at 519 ± 7 Ma (Hogmalm et al., 2017). In addition, the independent reference material GL-O gave an age of 96 ± 4 Ma, accurate to its published K–Ar age of 95 ± 1.5 Ma (Charbit et al., 1998; Derkowski et al., 2009). It should be noted that this age is younger than the tuff-horizon age of the GL-O host rock, dated at 113 ± 0.3 Ma (Selby, 2009). Consequently, the ages yielded from GL-O have instead been proposed to be indicative of the formation of glauconite occurring early after the deposition of the host rock (Selby, 2009).

Glass standard NIST SRM 610 was used as a primary standard for elemental quantification in this study. Analysis of secondary standard BCR-2G yielded major, trace and rare earth element composition that were in good agreement (Pearson R > 0.999, Pearson R^2 > 0.999, and P Value < 0.0001) with their published values as compiled in the GeoREM database (Jochum and Stoll, 2008; Jochum et al., 2011; Jochum et al., 2005; Pearce et al., 1997).

One-dimensional thermal modelling of the Altree 2 well was conducted using the SILLi 1.0 numerical model, which is designed for simulating thermal perturbation associated with sill emplacement within sedimentary basins (Iyer et al., 2018). First, palaeotemperatures were estimated from the compiled thermal maturity data (Disnar, 1986, 1994; Waliczek et al., 2021) following equations based on similar sedimentary systems that experienced a heating event due to burial and a subsequent igneous intrusion (Piedad-Sánchez et al., 2004). Forward modelling was then conducted to replicate maximum thermal conditions calculated in the well from the thermal maturity data, where palaeotemperatures suggest that the Wyworrie and Amungee Members experienced significant additional sedimentary cover in the Mesoproterozoic. During modelling, an additional 1.5 km of sedimentary rocks were added above the erosional unconformity now present above the McArthur Basin fill (Hall et al., 2021), while all post-Mesoproterozoic units were excluded. The upper contact of a sill with an initial temperature of 1150°C (Wang et al.,

2012)) was set at 2868 m, in accordance with adjusted burial depths during the Mesoproterozoic. As sill thickness is unconstrained within the Altree 2 well, multiple iterations were run with different thicknesses in order to establish the scenario able to best satisfy the thermal aureole extent observed in this well. From this, a sill thickness of 75 m was considered most appropriate, and is consistent with Derim Derim sill thicknesses of ~10–100 m commonly observed across the basin (Lanigan and Ledlie, 1990; Lanigan and Torkington, 1991; Ledlie and Maim, 1989; NTGS, 2014, 2015, 2016). Full modelling parameters and petrophysical properties are provided in the Supplementary Material Table S2 and Table S3.

4 Results

4.1 Compilation of legacy data

All legacy data are compiled in the Supplementary Material and were checked for quality before interpretation as several factors such as contamination of cuttings due to drilling fluid or poor organic content can make results unreliable (Carvajal-Ortiz and Gentzis, 2015; Dembicki Jr, 2009; Peters, 1986). Rock-Eval pyrolysis values were screened using the thresholds described by Hall et al. (2016). Data were subsequently excluded from interpretation if these criteria were not met. More than 90% of the data yielded S2 > 0.1 mg HC/g, indicating that they were sufficiently abundant in organic content to provide well-defined peaks for characterising T_{max} and Hydrogen Index. Importantly, compilation of Rock-Eval pyrolysis values were all internally consistent (e.g., Hydrogen Index = S2/TOC x 100). Next, there was no evidence of anomalously low T_{max} values (< 380°C) present. Extremely low T_{max} values are commonly a product of incorrect selection of the S2 peak by the program or the widening of the S1 peak from non-indigenous free hydrocarbons. T_{max} results compiled in this study ranges between 384°C to 502°C with a mean of 433°C (st. dev. = 17). TOC content in the Velkerri Formation varies from 0.07% to 8.07%, averaging at 2.25% (st. dev. = 2.26). Clay mineral crystallinity and size data sourced for this compilation were standardised for interlaboratory comparisons (Warr and Mählmann, 2015; Warr and Rice, 1994). Full width at half maximum values from Altree 2 shale samples were computationally remeasured as a secondary check (Capogreco, 2017; NTGS, 2010, 2012). Thirteen samples from the Velkerri Formation were analysed for their illite crystallinity. The Kübler Index for these shales range between 0.88 to 0.36, with decreasing values at depth and the lowest data originating from the Kalala Member. Methylphenanthrene distribution factor (MPDF), methylphenanthrene ratios (MPR), and

bitumen reflectance data collated from Jarrett et al. (2019a) and Revie et al. (2022) also displays an increasing trend down-hole.

4.2 Mineralogy of the Velkerri Formation

Eleven mineral phases were identified by bulk XRD analysis of the Velkerri Formation from Cox et al. (2016). The major mineral phases were quartz, kaolinite, illite, and orthoclase, which on average make up 90% of the total composition of the samples. Trace minerals include glauconite, montmorillonite, pyrite, magnetite, siderite, dolomite, and plagioclase. Our MLA mapping also identified these assemblages. Importantly, the two different methods categorised these minerals at similar abundances. However, results from MLA mapping also found other mineral assemblages not identified by bulk XRD analysis, including biotite, chlorite, clinochlore, apatite, and zircon. These differences could be due to the slightly different sub-intervals from which samples were analysed. Bulk XRD is a destructive procedure and therefore, the same section cannot be reused for *in situ* analysis. As a result, samples spaced 1 – 2 cm apart may yield different results. In addition, the targeted areas for MLA are often spatially localised and only based on 2D information. As such, they may not be representative for the bulk rock, making the comparison with XRD datasets difficult. The complete mineralogical abundance and correlations between results bulk XRD and MLA mapping are summarised in Table 1. Extensive petrographic descriptions of all samples can be found in the Supplementary Material.

4.3 Laser ablation data

Geochronological results yielded by samples from the Wyworrie and Amungee Members gave ages within error of each other. The sample from 415 m depth was dated at 1448 ± 81 Ma. Next, the mudstone analysed from 520 m depth yielded an age of 1434 ± 19 Ma. Thirdly, the shale sample studied from 696 m depth resulted in an age of 1411 ± 139 Ma. A Kalala Member shale chip from 938 m at depth was dated at 1322 ± 93 Ma. Another sample from this member, towards the boundary with the underlying Bessie Creek Sandstone at depth 1220 m resulted in an age of 1336 ± 40 Ma. The range of precision from these Rb–Sr ages are primarily constrained by a substantial spread in $^{87}Rb/^{86}Sr$ ratios, the number of data points defining the regression line as well as errors on each individual analysis (Nebel, 2014). The most precisely dated samples, extracted from 520 m and 1220 m depth, had the widest range of $^{87}Rb/^{86}Sr$ ratios (0 – 50) whilst the other two samples preserved a range of $^{87}Rb/^{86}Sr$ values less than 10 (Figure 6). The variability in these values could be a subject of future studies in order to improve the success of this dating

method. Single-spot ages were calculated for all spot analyses in each sample, and their populations categorically differ (Figure 8).

Elemental concentrations of each sample were concurrently collected during the *in situ* Rb–Sr laser ablation investigation and they are in good agreement with data collected by bulk geochemical analysis from Cox et al. (2016). Samples from depth 415 m, 520 m, and 696 m do not show any covariation between their total REEY concentrations and Sm/Nd ratios (Figure 7). On the other hand, sample 938 m showed a statistically significant relationship between these two parameters (Pearson R = 0.58, Pearson R^2 = 0.336, P Value < 0.0001). In addition, Velkerri Formation shale sourced from depth 1220 m also showed a strong covariation between total REEY values and Sm/Nd (Pearson R = -0.545, Pearson R^2 = 0.297, P Value < 0.0001). These associations were also identified in the whole-rock geochemical data collected from Cox et al. (2016). Figure 7B shows that samples between 390 – 900 m depth hold no statistically significant relationships between the two factors. However, samples from deeper than 900 m display a strong relationship between the two variables (Pearson R = -0.559, Pearson R^2 = 0.312, P Value = 0.003). The full geochronological and inorganic geochemical dataset for samples in this study can be found in the Supplementary Material.

4.4 Thermal Modelling

One-dimensional thermal modelling of the emplacement of a 75 m thick Derim Derim Dolerite sill at the base of the Altree 2 well is sufficient to produce a thermal aureole reaching temperatures > 110°C, ca. 800 m above the top contact of the sill (Figure 9A). Maximum palaeotemperatures recorded in the Wyworrie Members exceed those predicted in this simulation, however, this may be attributed to elevated temperatures in the shallow basin during eruption of the Kalkarindji LIP in the Cambrian (Nixon et al., 2022). The resultant maximum thermal profile is consistent with T_{max} derived palaeotemperature estimates and is thus considered a plausible model for the observed data from the well. Post-intrusion temperatures at depths that match the samples with reset Rb–Sr ages are much lower than observed in comparable isotopic systems for thermally induced diffusion (Dodson, 1973; Tillberg et al., 2020; Torgersen et al., 2015; Yoder and Eugster, 1955), with the shallowest reset sample peaking at ca. 120°C. Furthermore, elevated temperatures predicted by the modelling are geologically short lived, with temperatures returning to steady-state conditions by approximately half a million years following sill intrusion (Figure 9B).

Depth	Method	Apatite	Biotite	Chlorite	Dolomite	Glauconite	Illite	Kaolinite	Magnetite	Montmorillonite	Orthoclase	Pyrite	Quartz	Siderite	Zircon	Plagioclase
415 m	Bulk XRD	*0.00*	*0.00*	*0.00*	*0.25*	*0.82*	*34.05*	*21.25*	*0.36*	*1.79*	*13.33*	*0.28*	*26.13*	*1.76*	*0.00*	*0.00*
	MLA Map	*0.00*	*1.22*	*1.33*	*0.00*	*0.00*	*35.52*	*7.45*	*0.89*	*9.05*	*11.48*	*0.40*	*23.93*	*0.00*	*0.02*	*4.39*
520 m	Bulk XRD	*0.00*	*0.00*	*0.00*	*0.37*	*2.35*	*43.28*	*17.14*	*0.38*	*2.01*	*10.01*	*0.74*	*23.67*	*0.05*	*0.00*	*0.00*
	MLA Map	*0.00*	*0.07*	*0.08*	*0.00*	*0.00*	*36.51*	*7.11*	*0.00*	*0.04*	*4.08*	*0.24*	*47.94*	*0.00*	*0.00*	*0.85*
696 m	Bulk XRD	*0.00*	*0.00*	*0.00*	*0.21*	*1.53*	*27.59*	*2.07*	*0.00*	*1.49*	*13.40*	*4.11*	*45.02*	*0.00*	*0.00*	*4.57*
	MLA Map	*0.31*	*0.93*	*0.06*	*0.00*	*0.00*	*18.48*	*0.00*	*0.00*	*4.00*	*8.27*	*4.47*	*60.88*	*0.00*	*0.00*	*1.41*
938 m	Bulk XRD	*0.00*	*0.00*	*0.00*	*0.53*	*1.36*	*27.03*	*6.99*	*0.33*	*1.16*	*11.32*	*1.49*	*43.28*	*0.01*	*0.00*	*6.50*
	MLA Map	*1.2*	*0.00*	*0.06*	*0.00*	*0.00*	*22.13*	*5.46*	*0.00*	*0.00*	*3.37*	*1.60*	*57.79*	*0.00*	*0.00*	*6.90*
1220 m	Bulk XRD	*0.00*	*0.00*	*0.00*	*0.43*	*1.04*	*39.36*	*13.99*	*0.42*	*1.66*	*7.32*	*0.26*	*33.56*	*0.10*	*0.00*	*1.86*
	MLA Map	*0.00*	*0.01*	*0.01*	*0.05*	*0.00*	*38.18*	*20.21*	*0.00*	*0.00*	*4.45*	*0.01*	*35.25*	*0.00*	*0.01*	*1.63*

Depth (m)	Pearson R	Pearson R 95% C.I.	Pearson R^2	P Value
415	*0.922*	*0.784–0.973*	*0.850*	*< 0.0001*
520	*0.866*	*0.648–0.953*	*0.750*	*<0.0001*
696	*0.953*	*0.868–0.984*	*0.910*	*<0.0001*
938	*0.965*	*0.898–0.988*	*0.930*	*<0.0001*
1220	*0.989*	*0.969–0.996*	*0.979*	*<0.0001*

Table 1A. Mineralogical abundance of the Velkerri Formation shales collected by bulk XRD analysis from Cox et al. (2016) and spectral reflectance MLA mapping in this study. All values are in weight percent. B. Covariation between the mineral phases categorised by both methods.

5 Thermal Maturity of the Velkerri Formation

Geochemical and mineralogical-based thermal maturity indicators collected via Rock-Eval studies and bulk XRD analyses were compiled in this study in order to establish a vertical profile of the Velkerri Formation and assess the local palaeo-thermal structure. The T_{max} parameter is the temperature at which the maximum rate of hydrocarbon generation occurs during pyrolysis analysis and is a common method used to reconstruct thermal histories of basin systems (Espitalié, 1986; Espitalié et al., 1977; Peters and Cassa, 1994; Welte and Tissot, 1984). Additionally, the Kübler index (KI) is determined by the 001-reflection of illite and is also a popular maturation proxy used to classify low-grade metamorphism in pelitic rocks (Blenkinsop, 1988; Guggenheim et al., 2002; Kubler, 1967). However, both of these thermal indicators can be influenced by multiple factors other than burial-related heating and therefore struggle to resolve absolute quantitative palaeotemperatures. Changes in heating rate, abundance in hydrogen, sulphur, and uranium content or the organic richness of samples can result in inaccurate T_{max} values (Dembicki Jr, 2009; Espitalié et al., 1977; Peters, 1986; Yang and Horsfield, 2020). Similarly, the KI has also been shown to be sensitive to several parameters such as changes heating rate and geochemical variability in the sample's initial mineralogy (Abad and Nieto, 2007; Eberl and Velde, 1989; Mählmann et al., 2012; Warr and Mählmann, 2015). In addition, variations in procedures between laboratories can further complicate the direct comparison of these values (Cornford et al., 1998; Jarvie, 1991; Peters and Cassa, 1994; Tissot et al., 1987). Consequently, these thermal indicators need to be treated with caution when applied independently and are more suitable as qualitative

discriminators as opposed to absolute quantitative parameters. However, such proxies can be more confidently used to estimate palaeotemperatures in sedimentary successions if they show a strong relationship with each other (Burtner and Warner, 1986; Dellisanti et al., 2010; Ola et al., 2018; Velde and Espitalié, 1989; Waliczek et al., 2021). Ultimately, both organic and inorganic indicators are essential for a robust understanding of the thermal histories of sedimentary sequences through time.

In this study, we examine the covariation between the T_{max} values and KI to reconstruct the thermal history of the Velkerri Formation in the Altree 2 well (Figure 3). In our compilation, samples with immature kerogen (T_{max} < 435°C) correspond to rocks in the diagenetic zone (KI > 0.45°Δ2θ). This relationship is true in similar studies and generally translates to palaeotemperatures of ca. 100°C (Abad and Nieto, 2007; Dellisanti et al., 2010; Espitalié et al., 1977; Kosakowski et al., 1999; Kubler, 1967).

Interestingly, the samples within the mature oil window (435°C < T_{max} < 465°C) show a wide range of KI values between 0.39 and 0.65°Δ2θ (Figure 3). This is possibly due to the delay between thermal reactions in clay minerals as opposed to organic matter (Ola et al., 2018). Although the maturation of organic matter and the morphology of clay minerals both largely depend on temperature, other processes such as the kinetics of the thermal reaction and geochemical composition of the sample can make these relationships non-linear (Meunier et al., 2004; Ola et al., 2018; Pollastro, 1993; Varajao and Meunier, 1995; Velde and Vasseur, 1992). The disparity between kerogen evolution and the equilibrium stage of illitisation at these temperatures may also play a role in this variability (Dellisanti et al., 2010). Nevertheless, an increase in T_{max} pyrolysis results from these samples still appears to correlate with a decrease in KI values. These thermometers would approximately equate to palaeotemperatures between 100 and 150°C (Árkai et al., 2002; Frey and Merriman, 1999; Kosakowski et al., 1999; Welte and Tissot, 1984).

On the other hand, the sample displaying over-mature kerogen (T_{max} > 465°C) corresponds to the smallest KI value (Figure 3) of 0.36°Δ2θ (Dellisanti et al., 2010). These values commonly define the gas window and the anchizone, corresponding to palaeotemperatures of ca. 200°C (Árkai et al., 2002; Dellisanti et al., 2010; Kosakowski et al., 1999). Overall, a trend between increasing T_{max} and decreasing KI values (Figure 3) confirms the feasibility of these parameters as thermal maturation proxies (Dellisanti et al., 2010).

Lastly, the thermal parameters for the Velkerri Formation can be further examined by inspecting the changes in MPDF (Boreham et al., 1988; Kvalheim et al., 1987), MPR (Radke et al., 1982; Wilhelms et al., 1998), and bitumen reflectance (Riediger, 1993). Previous studies have shown that aromatic hydrocarbons were effective in providing thermal constraints for the Velkerri Formation (George and Ahmed, 2002b; Jarrett et al., 2019a). These proxies were similarly sensitive to maturity variations from thermally immature to late oil window. As such, we normalise the thermal indicators used in this study by converting them all (Jarrett et al., 2019a; Jarvie et al., 2001; Revie et al., 2022) to calculated vitrinite reflectance values (VR_{CALC}; Figure 4). The VR_{CALC} from four different thermal indicators show that the Velkerri Formation quickly elevated in maturity and enters the gas window at ca. 900 m depths (Figure 4). The agreement of all proxies add further confidence in the temperature constrains used in this study.

Multiple geochemical and mineralogical thermal parameters from our compiled data-set demonstrate strong correlation between them, suggesting that the proxies used in this study primarily recorded changes in palaeotemperature as opposed to other possible variables. Notably, five different, independent, source-rock maturation proxies statistically agree and recorded similar step-wise increase in thermal history down-hole. As such, we investigated five samples approaching the geothermal anomaly in the Kalala Member for *in situ* Rb–Sr and trace element analysis. The changes in thermal maturation indexes throughout the well are used to help constrain the parameters of the Rb–Sr isotopic system in Proterozoic shales.

6 Thermochronological History of the Velkerri Formation

Although some of the geochronological results of these samples may overlap due to their errors (Figure 6), they are still categorically different down-hole (Figure 8). We display these differences by plotting the population of single-spot ages from each sample against each other. Kernel Distribution Estimate (KDE) plots of these results show that the distribution of single-spot ages from samples shallower than 900 m largely overlaps with the Re–Os age constraint (Figure 8A; light pink) for the Velkerri Formation (Kendall et al., 2009). On the other hand, the population of single-spot ages from shales deeper than 900 m instead agree with the age for the Derim Derim Dolerite (Figure 8A; dark pink) intrusion ca. 1330–1300 Ma (Ahmad and Munson, 2013; Bodorkos et al., 2022; Nixon et al., 2021; Yang et al., 2020).

Importantly, these sample-sets are statistically different from each other. This is graphically shown by their cumulative age distribution (CAD, Figure 8B) and Multidimensional Scaling (MDS, Figure 8C) plots. The second of these techniques statistically measures the dissimilarity between different age distributions through the Kolmogorov-Smirnov test (Vermeesch, 2013). In short, similar age distributions will plot closely to each other whilst distributions that are increasingly dissimilar will plot further away (Vermeesch, 2012, 2013). Figure 8B and 8C show that samples shallower than 900 m had age distributions that are similar to each other (Figure 8). Overall, these ages are statistically similar to the Re–Os constraint of the Velkerri Formation (Kendall et al., 2009), suggesting that they likely represent an early diagenetic/burial age soon after deposition. On the other hand, the single-age distributions of samples deeper than 900 m are statistically different to the previous sample set. They form their own cluster, which in turn coincides with the age of the Derim Derim Dolerites (Ahmad and Munson, 2013; Bodorkos et al., 2022; Nixon et al., 2021; Yang et al., 2020). Consequently, the Rb–Sr shales ages from this section are unlikely to date the deposition of the Velkerri Formation, but instead reflect a late-stage hydrothermal resetting induced by the intrusion.

The petrographic characteristics of assemblages in these samples are further evidence that the shales in the Velkerri Formation recorded two distinct thermochronological events. The abundant clays in samples from depth 415 m, 520 m, and 696 m are predominantly illite, with trace amounts of chlorite, kaolinite, and montmorillonite (Table 1). However, they do not show typical irregular, angular detrital morphologies (Figure 5, Figure S2A-C). Instead, clay minerals in these samples form a matrix cement, filling in porous spaces, wrapping around detrital grains and suggesting that they formed within the sediment during burial diagenesis (Rafiei and Kennedy, 2019; Rafiei et al., 2020; Subarkah et al., 2021). Primary sedimentary structures such compaction of clays along the bedding plane can also still be identified in these samples (Figure 5, Figure S2A-C and Supplementary Material). These petrographic relationships are further discussed in the Supplementary Material and were similarly found in Roper Group shales elsewhere, indicating an early-diagenetic origin (Rafiei and Kennedy, 2019; Subarkah et al., 2021). Moreover, the ages from these samples are all in agreement with the deposition of the Velkerri Formation dated at 1417 ± 29 Ma by Re–Os geochronology (Kendall et al., 2009), suggesting that the majority of illite formed relatively soon after sediment deposition.

Nevertheless, we also sought to identify any potential secondary alteration of these shales by analysing their geochemical signatures. Sm/Nd ratios are common geochemical proxies for screening alteration in shales as Nd is preferentially lost relative to Sm during post-depositional processes (Awwiller and Mack, 1989; Awwiller and Mack, 1991). In addition, fluid-rock reactions also have a significant impact on rare earth element and yttrium solubility and transportation during hydrothermal events (Lev et al., 1999; Williams-Jones et al., 2012). Therefore, these parameters can be an effective tool for highlighting fingerprints of post-depositional geochemical mobilisation (Figure 7).

Samples from depths shallower than 900 m show no significant relationships between their total rare earth elements and yttrium (REEY) concentrations and Sm/Nd ratios collected by laser ablation analysis or through traditional bulk trace element geochemistry (Cox et al., 2016). These support an interpretation that these ages form a minimum depositional age for the unit, recording an early diagenetic event as opposed to a late-stage secondary overprint. Furthermore, temperature constrains for the Velkerri Formation at depths 390 – 900 m suggest that they are well-within the oil window (Figure 3 and 4). As a result, we propose that this temperature window is not sufficient to disturb the Rb–Sr and trace element systems in these shales.

Conversely, shales collected from depths >900 m showed petrographic evidence of post-depositional alteration (Figure 5 and Figure S2D-E). Clay minerals the 938 m sample are fissile and foliated (Figure 5). In addition, pyrite and apatite can be observed overgrowing illite and chlorite. Moreover, illite grains from the Kalala Member shale at 1220 m depth are notably larger and crystalline (Figure 5 and Figure S2D-E), with features inconsistent with an early diagenetic origin (and Figure S2D-E). Clay minerals were also found interlocking with quartz overgrowth and appear to replace earlier assemblages (Figure 5 and Figure S2D-E).

In addition to petrographic and geochronological disparities, samples from depths below 900 m display statistically significant relationships between total REEY concentrations and Sm/Nd ratios (Figure 7). The shale chip analysed from 938 m had a positive relationship between an increase in Sm/Nd ratio and total REEY concentration (Pearson r: 0.580, R-squared: 0.336), while the sample collected from depth 1220 m preserved a negative relationship between Sm/Nd ratio and total REEY values (Pearson r: -0.545, R-squared: 0.297). These associations are similarly reflected in the bulk trace element data collated from Cox et al. (2016). In the compiled data, shales from deeper than 900 m demonstrate a strong affinity between these controls (Pearson r: -0.559, R-squared: 0.312). These

alteration indicators are further evidence that the Kalala Member at depths below 900 m experienced a late-stage secondary heating event, as trace elements are more readily mobilised in hydrothermal reactions (Awwiller and Mack, 1989; Awwiller and Mack, 1991; Condie, 1991; Lev et al., 1999; Poitrasson et al., 1995; Williams-Jones et al., 2012).

Importantly, thermal indicators from this interval suggest that kerogen in these shales are thermally overmature (Figure 3 and 4). Previous studies have shown that the source rocks in the Velkerri Formation became overmature only when affected by magmatic events (Crick et al., 1988; George and Ahmed, 2002a). As such, it is plausible that the Derim Derim Dolerite intersected in this well has imposed a hydrothermal alteration footprint onto the surrounding sediments via conductive heat loss and/or heat-transfer fluids. This magmatic pulse would have recrystallised the former mineral assemblages or induced a second mineralisation of clays, mobilised trace elements, and heated the kerogen within the Kalala Member to overmaturity. Thermal indicators (Figure 4 and 9) suggest that source-rocks within this interval may have experienced palaeotemperatures of at least 150°C (Dellisanti et al., 2010; Frey and Merriman, 1999; Hunt, 1995; Welte and Tissot, 1984). This is in good agreement with evidence from aqueous fluid inclusions in quartz veins within the Derim Derim Dolerite elsewhere, which have suggested that hydrocarbons from the Velkerri Formation migrated in the cooling sill at similar temperatures (Dutkiewicz et al., 2004). Importantly, such hydrothermal systems seem to be sufficient for disturbing the Rb–Sr isotopic system of these samples.

7 Modelled Predictions of the Geothermal Aureole Induced by the Derim Derim Dolerite

Resetting of Rb–Sr geochronology and overmaturation of hydrocarbons in the Kalala Member within the Altree 2 well implies the presence of a secondary hydrothermal aureole extending ca. 800 m away from the Derim Derim Dolerite sill, which is intersected at present day depth 1696 m. One-dimensional thermal modelling for a sill thickness of 75 m in the Mesoproterozoic suggests temperatures exceeding the oil window over 120°C (Tissot et al., 1974; Waples, 1980) only extended ca. 700 m from the intrusion (Figure 9A).

Samples at present day depths of 938 m and 1220 m yield Rb–Sr ages corresponding to emplacement timing of the Derim Derim Dolerite (Nixon et al., 2021; Yang et al., 2020), which suggests that the intrusion caused the chronometer to reset or induced a second mineralisation of clay phases. Predicted temperatures experienced by the shallowest reset sample, however, are lower than the inferred closure temperatures for observed K–Ar and Rb–Sr in

sheet silicates (Dodson, 1973; Tillberg et al., 2020; Torgersen et al., 2015; Yoder and Eugster, 1955). In a scenario in which a sill of thickness 75 m was intruded below samples, rocks from present day depth of 938 m are only predicted to have experienced maximum heating to ca. 110°C (Figure 9C), with temperatures exceeding 100°C for a duration of only ca. 150 ka (Figure 9B).

Additionally, the eruption of lavas from the Kalkarindji LIP (Evins et al., 2009; Glass and Phillips, 2006; Jourdan et al., 2014), within the same vertical profile offer an intriguing opportunity to evaluate thermal resistance of the Rb–Sr system in shale-hosted clays in different conditions. Basaltic lavas of the ca. 510 Ma Cambrian Kalkarindji LIP (Evins et al., 2009; Glass and Phillips, 2006; Jourdan et al., 2014) are preserved above Proterozoic sedimentary rocks in the Altree 2 well. Furthermore, regional apatite fission track data suggest that the thermal pulse induced during this LIP extrusion were short-lived but sufficient (> 190°C) to anneal tracks in the upper ~500 m of the basin (Nixon et al., 2022). However, the shallowest samples taken in this study (at depths 415 m, 520 m, and 696 m) did not have their Rb–Sr isotopic system disturbed despite experiencing such temperatures from this reheating event. Consequently, the thermal profile for the sample at 415 m depth provides a minimum closure temperature constraint for short-lived conditions which have not reset the Rb–Sr chronometer in these (presumably) dry shales over 800 million years after the Derim Derim dolerite intrusion. Interestingly, the Cambrian palaeotemperatures imposed by the Kalkarindji lavas (Nixon et al., 2022) are notably higher (> 190°C) than Mesoproterozoic palaeotemperatures reached by samples with Rb–Sr ages reset by the Derim Derim Dolerite (ca. 120°C; Figure 9A and 9B).

Such disparity suggests that the presence of fluid (either connate, or sourced from the intrusion), rather than just temperature, is likely to play a critical role in determining whether the Rb–Sr record in a shale is reset. As such, the geochemical system in shales within the aureole may be disturbed at lower temperatures, as trace and rare earth elements are more easily mobilised in hydrothermal fluid systems (Li et al., 2019; Nebel, 2014; Poitrasson et al., 1995; Villa, 1998; Williams-Jones et al., 2012).

8 Conclusion

We show that the Velkerri Formation shales intersected by the Altree 2 well preserve evidence of an elevated Mesoproterozoic thermal gradient through an ~800 m thick section away from the intrusion of a Derim Derim Dolerite sill (Figure 3, 4, and 9). *In situ* Rb–Sr isotopic ages from the Wyworrie and Amungee Members above this hydrothermal aureole yielded ages (Figure 6 and 8) within error of their depositional age (Kendall et al., 2009). In

addition, unaltered trace element compositions (Figure 7) and petrographic relationships indicate that the shales preserve an early-diagenetic origin (Figure 5 and Supplementary Material). However, the older Kalala Member that lies within the hydrothermal aureole yielded younger Rb–Sr ages (Figure 6 and 8) consistent with the age of the Derim Derim Dolerite (Ahmad and Munson, 2013; Bodorkos et al., 2022; Nixon et al., 2021; Yang et al., 2020). Samples from this subset also recorded perturbed trace element signatures (Figure 7) as well as fissile, foliated, and crystalline illite morphologies (Figure 5 and Supplementary Material). This interval corresponds with disturbed thermal maturity indicators (Figure 2, 3, and 4), suggesting that the Rb–Sr system is stable up to the maturation oil window and reset when the kerogen is overmature. Thermal modelling of the Derim Derim Dolerite suggests that a 75 m thick intrusion at the base of the Altree 2 well would have significantly elevated temperatures within 800 m of the sill, driving kerogen into the gas window, mobilising trace elements and resetting the Rb–Sr isotopic system in the Kalala Member.

In conclusion, we show that the *in situ* Rb–Sr dating of the Velkerri Formation combined with common hydrocarbon maturity proxies can help reveal the thermochronological history of Proterozoic argillaceous rocks. When used in tandem, these methods can constrain the age of deposition as well as subsequent secondary, late-stage geological events. Importantly, we demonstrate that this technique can aid sedimentary-hosted resource exploration, as hydrothermal overprints can be identified and dated as previously demonstrated in Subarkah et al. (2021). Specifically, for hydrocarbon exploration, we show that the thermo-kinetic parameters of shale-hosted Rb–Sr isotopic system in hydrothermal settings can coincide with the maturation of kerogen into the gas window (Dodson, 1973; Espitalié, 1986; Kubler, 1967).

9 Figure Captions

Figure 1A, left. Schematic stratigraphy and geochronological summary of the Roper Group (Abbott et al., 2001; Jackson et al., 1999; Kendall et al., 2009; Southgate et al., 2000; Subarkah et al., 2021; Yang et al., 2020). B, right. Sample location and depth to basement map for the McArthur Basin adapted from Frogtech Geoscience (2018).

Figure 2. Summary of reprocessed down-hole well log data for Altree 2.

Figure 3. Covariation between T_{max} values from pyrolysis analysis and illite crystallinity KI in the Velkerri Formation. An increase in T_{max} coincide with a decrease in KI, suggesting that these proxies are both mainly sensitive to changes in palaeotemperature.

Figure 4. Calculated vitrinite reflectance (VR_{CALC}) data down-hole modelled from T_{Max}, MPR, MPDF, and bitumen reflectance data compiled in this study (Capogreco, 2017; Cox et al., 2016; Jarrett et al., 2019b; Lemiux, 2011; NTGS, 1989, 2009, 2010, 2012; Revie, 2014; Revie et al., 2022). VR_{CALC} from all proxies all indicate an elevation in thermal maturity into the gas window at depths ca. 900 m.

Figure 5. Spectral reflectance MLA maps of samples selected for *in situ* laser ablation analysis in this study overlain on top of their respective BSE images. White dash lines show illite assemblages wrapping around detrital grains and forming cements. Black dash lines show foliation in illite crystals. Black dashed lines show large illite crystals replacing previous clay assemblages. Solid white lines are 100 µm scale bars.

Figure 6. Summary of *in situ* Rb–Sr geochronological results from this study.

Figure 7. Statistical relationships between alteration proxies obtained from this study through laser ablation analysis (A) and whole-rock geochemical data (B) compiled from Cox et al. (2016).

Figure 8. Single-spot ages from samples in this study illustrated by KDE (A), CAD (B), and MDS (C) plots. Note that the population of single-spot ages for samples at depths 415 m, 520 m, and 696 m all overlap with previous Velkerri Formation Re–Os age constraints shown in light pink (Kendall et al., 2009). On the other hand, samples at depth 938 m, and 1220 m are statistically different and instead agree with the Derim Derim Dolerite intrusion ca. 1330–1300 Ma displayed in dark pink (Bodorkos et al., 2022).

Figure 9A. One-dimensional thermal model for sill intrusion of 75 m thickness within the Altree 2 well depicting time steps following emplacement at 0 ka. Sill intrusion and Rb–Sr sample depths have been normalised to palaeodepths with 1.5 km of additional Mesoproterozoic sediments (Hall et al., 2021). Median palaeotemperature estimates from VR_{CALC} data from the Altree 2 well have been included for comparison to modelled temperatures. B. Time-temperature profile for sample intervals within the Altree 2 well following intrusions of a sill of 75 m thick.

10 Acknowledgments

This work was supported by the Australian Research Council Projects LP160101353 and LP200301457 with Santos Ltd, Empire Energy Group Ltd, Northern Territory Geological Survey, Teck Resources, BHP, and Origin as partners. The initial development and validation of *in situ* Rb–Sr dating technique at the University of Adelaide was also supported by Agilent Technologies Australia Ltd. This manuscript forms MinEx CRC contribution #2022/60. Aoife McFadden is thanked for their assistance in the MLA mapping of the samples in this study. Jarred Lloyd is thanked for his help in the laser data processing. Jarred Lloyd's code to process error correlations on LADR can be found in https://github.com/jarredclloyd/PowerShell_LADR_errorcorrelation_workaround.

11 Author Contributions

Darwinaji Subarkah (primary author): Conceptualisation, method development, experimentation, manuscript drafting.

Angus Leslie Nixon: Conceptualisation, computational modelling, manuscript drafting.

Monica Jimenez: Conceptualisation, manuscript drafting.

Alan Stephen Collins: Conceptualisation, primary supervision, manuscript drafting, funding.

Morgan Lee Blades: Sampling, method development, experimentation, manuscript drafting, secondary supervision.

Juraj Farkaš: Conceptualisation, method development, secondary supervision.

Sarah Gilbert: Method development, experimentation, manuscript drafting.

Simon Holford: Manuscript drafting, conceptualisation.

Amber Jarrett: Manuscript drafting, data collection.

12 Competing Interests

The authors declare that they have no conflict of interest.

13 References Cited

Abad, I., and Nieto, F., 2007, Physical meaning and applications of the illite Kübler index: measuring reaction progress in low-grade metamorphism: Diagenesis and Low-Temperature Metamorphism, Theory, Methods and Regional Aspects, Seminarios. Sociedad Espanola: Sociedad Espanola Mineralogia, p. 53-64.

Abbott, S. T., and Sweet, I. P., 2000, Tectonic control on third-order sequences in a siliciclastic ramp-style basin: An example from the Roper Superbasin (Mesoproterozoic), northern Australia: Australian Journal of Earth Sciences, v. 47, no. 3, p. 637-657.

Abbott, S. T., Sweet, I. P., Plumb, K. A., Young, D. N., Cutovinos, A., Ferenczi, P. A., and Pietsch, B. A., 2001, Roper Region: Urapunga and Roper River Special, Northern Territory (Second Edition). 1:250000 geological map series explanatory notes, SD 53-10, 11.: Northern Territory Geological Survey and Geoscience Australia.

Ahmad, A., and Munson, T. J., 2013, Geology and mineral resources of the Northern Territory, Northern Territory Geological Survey, Special Publication.

Árkai, P., Sassi, F., and Desmons, J., 2002, Towards a unified nomenclature in metamorphic petrology: 4: Very low-to low-grade metamorphic rocks. A proposal on behalf of the IUGS Subcommission on the Systematics of Metamorphic Rocks. Web version of.

Armistead, S. E., Collins, A. S., Redaa, A., Jepson, G., Gillespie, J., Gilbert, S., Blades, M. L., Foden, J. D., and Razakamanana, T., 2020, Structural evolution and medium-temperature thermochronology of central Madagascar: implications for Gondwana amalgamation: Journal of the Geological Society, p. jgs2019-2132.

Awwiller, D. N., and Mack, L. E., 1989, Diagenetic Resetting of Sm-Nd Isotope Systematics in Wilcox Group Sandstones and Shales, San Marcos Arch, South-Central Texas: AAPG Bulletin, v. 39.

Awwiller, D. N., and Mack, L. E., 1991, Diagenetic modification of Sm-Nd model ages in Tertiary sandstones and shales, Texas Gulf Coast: Geology, v. 19, no. 4, p. 311-314.

Baldermann, A., Abdullayev, E., Taghiyeva, Y., Alasgarov, A., and Javad-Zada, Z., 2020, Sediment petrography, mineralogy and geochemistry of the Miocene Islam Dağ Section (Eastern Azerbaijan): Implications for the evolution of sediment provenance, palaeo-environment and (post-) depositional alteration patterns: Sedimentology, v. 67, no. 1, p. 152-172.

Bevan, D., Coath, C. D., Lewis, J., Schwieters, J., Lloyd, N., Craig, G., Wehrs, H., and Elliott, T., 2021a, In situ Rb–Sr dating by collision cell, multicollection inductively-coupled plasma mass-spectrometry with pre-cell mass-filter, (CC-MC-ICPMS/MS): Journal of Analytical Atomic Spectrometry, v. 36, no. 5, p. 917-931.

Bevan, D., Coath, C. D., Lewis, J., Schwieters, J., Lloyd, N., Craig, G., Wehrs, H., and Elliott, T., 2021b, In situ Rb–Sr dating by collision cell, multicollection inductively-coupled plasma mass-spectrometry with pre-cell mass-filter,(CC-MC-ICPMS/MS): Journal of analytical atomic spectrometry, v. 36, no. 5, p. 917-931.

Blenkinsop, T. G., 1988, Definition of low-grade metamorphic zones using illite crystallinity: Journal of Metamorphic Geology, v. 6, no. 5, p. 623-636.

Bodorkos, S., Crowley, J. L., Claoué-Long, J. C., Anderson, J. R., and Magee, C. W., 2022, Precise U–Pb baddeleyite dating of the Derim Derim Dolerite, McArthur Basin, Northern Territory: old and new SHRIMP and ID-TIMS constraints: Australian Journal of Earth Sciences, p. 1-15.

Boreham, C., Crick, I., and Powell, T., 1988, Alternative calibration of the Methylphenanthrene Index against vitrinite reflectance: Application to maturity measurements on oils and sediments: Organic Geochemistry, v. 12, no. 3, p. 289-294.

Brown, D. A., Simpson, A., Hand, M., Morrissey, L. J., Gilbert, S., Tamblyn, R., and Glorie, S., 2022, Laser-ablation Lu-Hf dating reveals Laurentian garnet in subducted rocks from southern Australia: Geology, v. 50, no. 7, p. 837-842.

Burtner, R. L., and Warner, M. A., 1986, Relationship between illite/smectite diagenesis and hydrocarbon generation in Lower Cretaceous Mowry and Skull Creek shales of the northern Rocky Mountain area: Clays and Clay Minerals, v. 34, no. 4, p. 390-402.

Capogreco, N., 2017, Provenance and thermal history of the Beetaloo Basin using illite crystallinity and zircon geochronology and trace element data.

Carvajal-Ortiz, H., and Gentzis, T. J. I. J. o. C. G., 2015, Critical considerations when assessing hydrocarbon plays using Rock-Eval pyrolysis and organic petrology data: Data quality revisited, v. 152, p. 113-122.

Chamley, H., 1989, Clay formation through weathering, Clay sedimentology, Springer, p. 21-50.

Charbit, S., Guillou, H., and Turpin, L., 1998, Cross calibration of K–Ar standard minerals using an unspiked Ar measurement technique: Chemical Geology, v. 150, no. 1-2, p. 147-159.

Charlier, B. L., Ginibre, C., Morgan, D., Nowell, G. M., Pearson, D., Davidson, J. P., and Ottley, C., 2006, Methods for the microsampling and high-precision analysis of strontium and rubidium isotopes at single crystal scale for petrological and geochronological applications: Chemical Geology, v. 232, no. 3-4, p. 114-133.

Chen, J., Blume, H.-P., and Beyer, L., 2000, Weathering of rocks induced by lichen colonization—a review: Catena, v. 39, no. 2, p. 121-146.

Condie, K. C., 1991, Another look at rare earth elements in shales: Geochimica et Cosmochimica Acta, v. 55, no. 9, p. 2527-2531.

Cornford, C., Gardner, P., and Burgess, C., 1998, Geochemical truths in large data sets. I: Geochemical screening data: Organic Geochemistry, v. 29, no. 1-3, p. 519-530.
Cox, G. M., Collins, A. S., Jarrett, A. J., Blades, M. L., Shannon, A. V., Yang, B., Farkas, J., Hall, P. A., O'Hara, B., and Close, D. J. A. B., 2022, A very unconventional hydrocarbon play: the Mesoproterozoic Velkerri Formation of northern Australia, no. 20,220,110.
Cox, G. M., Jarrett, A., Edwards, D., Crockford, P. W., Halverson, G. P., Collins, A. S., Poirier, A., and Li, Z.-X., 2016, Basin redox and primary productivity within the Mesoproterozoic Roper Seaway: Chemical Geology, v. 440, p. 101-114.
Cox, G. M., Sansjofre, P., Blades, M. L., Farkas, J., and Collins, A. S., 2019, Dynamic interaction between basin redox and the biogeochemical nitrogen cycle in an unconventional Proterozoic petroleum system: Sci Rep, v. 9, no. 1, p. 5200.
Crick, I., Boreham, C., Cook, A., and Powell, T., 1988, Petroleum geology and geochemistry of Middle Proterozoic McArthur Basin, northern Australia II: Assessment of source rock potential: AAPG bulletin, v. 72, no. 12, p. 1495-1514.
Cuadros, J., 2017, Clay minerals interaction with microorganisms: a review: Clay Minerals, v. 52, no. 2, p. 235-261.
Deepak, A., Löhr, S., Abbott, A. N., Han, S., Wheeler, C., and Sharma, M., Testing the Precambrian reverse weathering hypothesis using a 1-billion-year record of marine shales, *in* Proceedings 2022 Goldschmidt Conference2022, GOLDSCHMIDT.
Dellisanti, F., Pini, G. A., and Baudin, F., 2010, Use of T max as a thermal maturity indicator in orogenic successions and comparison with clay mineral evolution: Clay minerals, v. 45, no. 1, p. 115-130.
Dembicki Jr, H., 2009, Three common source rock evaluation errors made by geologists during prospect or play appraisals: AAPG bulletin, v. 93, no. 3, p. 341-356.
Derkowski, A., Środoń, J., Franus, W., Uhlík, P., Banaś, M., Zieliński, G., Čaplovičová, M., and Franus, M., 2009, Partial dissolution of glauconitic samples: Implications for the methodology of K-Ar and Rb-Sr dating: Clays and Clay Minerals, v. 57, no. 5, p. 531-554.
Dickin, A. P., 2018, Radiogenic isotope geology, Cambridge university press.
Disnar, J. R., 1986, Détermination de paléotempératures maximales d'enfouissement de sédiments charbonneux à partir de données de pyrolyse, v. 303, no. 8, p. 691-696.
Disnar, J.R., 1994, Determination of maximum paleotemperatures of burial (MPTB) of sedimentary rocks from pyrolysis data on the associated organic matter: basic principles and practical application: Chemical Geology, v. 118, no. 1, p. 289-299.
Dodson, M. H., 1973, Closure temperature in cooling geochronological and petrological systems: Contributions to Mineralogy and Petrology, v. 40, no. 3, p. 259-274.
Duddy, I., Green, P., Gibson, H., and Hegarty, K., 2004, Regional Palaeothermal episodes in Northern Australia: Timor Sea Petrol. Geosci. (Proc. Timor Sea Symp. 2003).
Dutkiewicz, A., Volk, H., Ridley, J., and George, S. C., 2004, Geochemistry of oil in fluid inclusions in a middle Proterozoic igneous intrusion: implications for the source of hydrocarbons in crystalline rocks: Organic Geochemistry, v. 35, no. 8, p. 937-957.
Eberl, D., and Velde, B., 1989, Beyond the Kubler index: Clay minerals, v. 24, no. 4, p. 571-577.
Espitalié, J., 1986, Use of Tmax as a maturation index for different types of organic matter: comparison with vitrinite reflectance: Collection colloques et séminaires-Institut français du pétrole, no. 44, p. 475-496.

Espitalié, J., Madec, M., Tissot, B., Mennig, J., and Leplat, P., Source rock characterization method for petroleum exploration, *in* Proceedings Offshore Technology Conference1977, OnePetro.

Evins, L. Z., Jourdan, F., and Phillips, D. J. L., 2009, The Cambrian Kalkarindji Large Igneous Province: Extent and characteristics based on new 40Ar/39Ar and geochemical data, v. 110, no. 1-4, p. 294-304.

Faure, G., 1977, Principles of isotope geology.

Field, D., and Råheim, A., 1979, A geologically meaningless Rb–Sr total rock isochron: Nature, v. 282, no. 5738, p. 497-499.

Frey, R. M. M., and Merriman, R., 1999, Patterns of very low-grade metamorphism in metapelitic rocks M: Frey D. Robinson Low-Grade Metamorphism Blackwell Science Oxford, v. 61, p. 107.

Frogtech Geoscience, N. T. G. S., Digital Information Package, DIP, 2018, SEEBASE® study and GIS for greater McArthur Basin, v. 17.

Galán, E., 2006, Genesis of clay minerals: Developments in clay science, v. 1, p. 1129-1162.

George, S., and Ahmed, M., 2002a, Use of aromatic compound distributions to evaluate organic maturity of the Proterozoic middle Velkerri Formation, McArthur Basin, Australia.

George, S., and Ahmed, M., 2002b, Use of aromatic compound distributions to evaluate organic maturity of the Proterozoic middle Velkerri Formation, McArthur Basin, Australia.

Glass, L. M., and Phillips, D. J. G., 2006, The Kalkarindji continental flood basalt province: A new Cambrian large igneous province in Australia with possible links to faunal extinctions, v. 34, no. 6, p. 461-464.

Gorojovsky, L., and Alard, O., 2020, Optimisation of laser and mass spectrometer parameters for the in situ analysis of Rb/Sr ratios by LA-ICP-MS/MS: Journal of Analytical Atomic Spectrometry, v. 35, no. 10, p. 2322-2336.

Govindaraju, K., Rubeska, I., and Paukert, T., 1994, 1994 Report On Zinnwaldite Zw-C Analysed By Ninety-Two Git-Iwg Member-Laboratories: Geostandards Newsletter, v. 18, no. 1, p. 1-42.

Guggenheim, S., Bain, D. C., Bergaya, F., Brigatti, M. F., Drits, V. A., Eberl, D. D., Formoso, M. L., Galán, E., Merriman, R. J., and Peacor, D. R., 2002, Report of the Association Internationale pour l'Etude des Argiles (AIPEA) Nomenclature Committee for 2001: order, disorder and crystallinity in phyllosilicates and the use of the ‘crystallinity index’: Clay Minerals, v. 37, no. 2, p. 389-393.

Hahn, O., Strassman, F., Mattauch, J., and Ewald, H., 1943, Geologische Altersbestimmungen mit der strontiummethode: Chem. Zeitung, v. 67, p. 55-56.

Hahn, O., and Walling, E., 1938, Über die Möglichkeit geologischer Altersbestimmungen rubidiumhaltiger Mineralien und Gesteine: Zeitschrift für anorganische und allgemeine Chemie, v. 236, no. 1, p. 78-82.

Hall, L., Boreham, C. J., Edwards, D. S., Palu, T., Buckler, T., Troup, A., and Hill, A., 2016, Cooper Basin Source Rock Geochemistry, Geoscience Australia.

Hall, L. S., Orr, M. L., Lech, M. E., Lewis, S., Bailey, A. H. E., Owens, R., Bradshaw, B. E., and Bernardel, G., 2021, Geological and Bioregional Assessments: assessing the prospectivity for tight, shale and deep-coal resources in the Cooper Basin, Beetaloo Subbasin and Isa Superbasin: The APPEA Journal, v. 61, no. 2, p. 477-484.

Harrison, T. M., Heizler, M. T., McKeegan, K. D., and Schmitt, A. K., 2010, In situ 40K–40Ca 'double-plus' SIMS dating resolves Klokken feldspar 40K–40Ar paradox: Earth and Planetary Science Letters, v. 299, no. 3-4, p. 426-433.

Hillier, S., 1995, Erosion, sedimentation and sedimentary origin of clays, Origin and mineralogy of clays, Springer, p. 162-219.

Hogmalm, K. J., Dahlgren, I., Fridolfsson, I., and Zack, T., 2019, First in situ Re-Os dating of molybdenite by LA-ICP-MS/MS: Mineralium Deposita, v. 54, no. 6, p. 821-828.

Hogmalm, K. J., Zack, T., Karlsson, A. K. O., Sjöqvist, A. S. L., and Garbe-Schönberg, D., 2017, In situ Rb–Sr and K–Ca dating by LA-ICP-MS/MS: an evaluation of N2O and SF6 as reaction gases: Journal of Analytical Atomic Spectrometry, v. 32, no. 2, p. 305-313.

Hunt, J. M., 1995, Petroleum geochemistry and geology.

Isson, T. T., and Planavsky, N. J., 2018, Reverse weathering as a long-term stabilizer of marine pH and planetary climate: Nature, v. 560, no. 7719, p. 471-475.

Iyer, K., Svensen, H., and Schmid, D. W., 2018, SILLi 1.0: a 1-D numerical tool quantifying the thermal effects of sill intrusions: Geosci. Model Dev., v. 11, no. 1, p. 43-60.

Jackson, M., Sweet, I., Page, R., and Bradshaw, B., 1999, The South Nicholson and Roper Groups: evidence for the early Mesoproterozoic Roper Superbasin: Integrated Basin Analysis of the Isa Superbasin using Seismic, Well-log, and Geopotential Data: An Evaluation of the Economic Potential of the Northern Lawn Hill Platform: Canberra, Australia, Australian Geological Survey Organisation Record, v. 19.

Jackson, M. J., Muir, M. D., Plumb, K. A., Australia. Bureau of Mineral Resources, G., and Geophysics, 1987, Geology of the Southern McArthur Basin, Northern Territory, Australian Government Pub. Service.

Jarrett, A. J., Cox, G. M., Brocks, J. J., Grosjean, E., Boreham, C. J., and Edwards, D. S., 2019a, Microbial assemblage and palaeoenvironmental reconstruction of the 1.38 Ga Velkerri Formation, McArthur Basin, northern Australia: Geobiology, v. 17, no. 4, p. 360-380.

Jarrett, A. J. M., Cox, G. M., Brocks, J. J., Grosjean, E., Boreham, C. J., and Edwards, D. S., 2019b, Microbial assemblage and palaeoenvironmental reconstruction of the 1.38 Ga Velkerri Formation, McArthur Basin, northern Australia: Geobiology, v. 17, no. 4, p. 360-380.

Jarvie, D. M., 1991, Factors affecting Rock-Eval derived kinetic parameters: Chemical Geology, v. 93, no. 1-2, p. 79-99.

Jarvie, D. M., Claxton, B. L., Henk, F., and Breyer, J. T., Oil and shale gas from the Barnett Shale, Ft, in Proceedings Worth Basin, Texas (abs.): AAPG Annual Meeting Program2001, Volume 10, p. A100.

Jenkin, G. R., Rogers, G., Fallick, A. E., and Farrow, C. M., 1995, Rb・Sr closure temperatures in bi-mineralic rocks: a mode effect and test for different diffusion models: Chemical Geology, v. 122, no. 1-4, p. 227-240.

Jochum, K., and Stoll, B., 2008, Reference materials for elemental and isotopic analyses by LA-(MC)-ICP-MS: Successes and outstanding needs: Laser ablation ICP-MS in the Earth sciences: Current practices and outstanding issues, 147-168 (2008), v. 40.

Jochum, K. P., Weis, U., Stoll, B., Kuzmin, D., Yang, Q., Raczek, I., Jacob, D. E., Stracke, A., Birbaum, K., Frick, D. A., Günther, D., and Enzweiler, J., 2011, Determination of Reference Values for NIST SRM 610–617 Glasses Following ISO Guidelines: Geostandards and Geoanalytical Research, v. 35, no. 4, p. 397-429.

Jochum, K. P., Willbold, M., Raczek, I., Stoll, B., and Herwig, K., 2005, Chemical Characterisation of the USGS Reference Glasses GSA-1G, GSC-1G, GSD-1G, GSE-1G, BCR-2G, BHVO-2G and BIR-1G Using EPMA, ID-TIMS, ID-ICP-MS and LA-ICP-MS: Geostandards and Geoanalytical Research, v. 29, no. 3, p. 285-302.

Jourdan, F., Hodges, K., Sell, B., Schaltegger, U., Wingate, M., Evins, L., Söderlund, U., Haines, P., Phillips, D., and Blenkinsop, T. J. G., 2014, High-precision dating of the Kalkarindji large igneous province, Australia, and synchrony with the Early–Middle Cambrian (Stage 4–5) extinction, v. 42, no. 6, p. 543-546.

Kendall, B., Creaser, R., Gordon, G., and Anbar, A., 2009, Re-Os and Mo isotope systematics of black shales from the Middle Proterozoic Velkerri and Wollogorang Formations, McArthur Basin, northern Australia: Geochimica et Cosmochimica Acta, v. 73, p. 2534-2558.

Kennedy, M., Droser, M., Mayer, L. M., Pevear, D., and Mrofka, D., 2006, Late Precambrian oxygenation; inception of the clay mineral factory: Science, v. 311, no. 5766, p. 1446-1449.

Kosakowski, G., Kunert, V., Clauser, C., Franke, W., and Neugebauer, H. J., 1999, Hydrothermal transients in Variscan crust: paleo-temperature mapping and hydrothermal models: Tectonophysics, v. 306, no. 3, p. 325-344.

Kubler, B., 1967, La cristallinité de l'illite et les zones tout à fait supérieures du métamorphisme: Etages tectoniques, p. 105-121.

Kvalheim, O. M., Christy, A. A., Telnæs, N., and Bjørseth, A., 1987, Maturity determination of organic matter in coals using the methylphenanthrene distribution: Geochimica et Cosmochimica Acta, v. 51, no. 7, p. 1883-1888.

Lanigan, K., and Ledlie, I. M., 1990, Walton-1,2 EP 24 McArthur Basin, Northern Territory Well Completion Report: Pacific Oil and Gas, PR1989-0088.

Lanigan, K., and Torkington, J., 1991, Well Completion Report EP19 - Sever 1, Daly Sub-basin of the McArthur Basin: Pacific Oil and Gas, PR1990-0069.

Laureijs, C. T., Coogan, L. A., and Spence, J., 2021a, In-situ Rb-Sr dating of celadonite from altered upper oceanic crust using laser ablation ICP-MS/MS: Chemical Geology, v. 579, p. 120339.

Laureijs, C. T., Coogan, L. A., and Spence, J., 2021b, In-situ RbSr dating of celadonite from altered upper oceanic crust using laser ablation ICP-MS/MS: Chemical Geology, p. 120339.

Ledlie, I. M., and Maim, K., 1989, Lawrence 1 EP 5 McArthur Basin, Northern Territory Well Completion Report: Pacific Oil and Gas, PR1989-0005.

Lee, M., and Parsons, I., 1999, Biomechanical and biochemical weathering of lichen-encrusted granite: textural controls on organic–mineral interactions and deposition of silica-rich layers: Chemical Geology, v. 161, no. 4, p. 385-397.

Lemiux, Y., 2011, Altree 2, Burdo 1, Chanin 1, Jamison 1, McManus 1, Shenandoah 1A, Walton 2, Balmain-1, Elliott-1 pyrolysis and tight rock analysis: Talisman Energy, Advanced Well Technologies,
Northern Territory Geological Survey, CSR0192

Lev, S. M., McLennan, S. M., and Hanson, G. N., 1999, Mineralogic controls on REE mobility during black-shale diagenesis: Journal of Sedimentary Research, v. 69, no. 5, p. 1071-1082.

Li, S.-S., Santosh, M., Farkaš, J., Redaa, A., Ganguly, S., Kim, S. W., Zhang, C., Gilbert, S., and Zack, T., 2020, Coupled U-Pb and Rb-Sr laser ablation geochronology trace Archean to Proterozoic crustal evolution in the Dharwar Craton, India: Precambrian Research, v. 343, p. 105709.

Li, S., Wang, X.-C., Li, C.-F., Wilde, S. A., Zhang, Y., Golding, S. D., Liu, K., and Zhang, Y., 2019, Direct Rubidium-Strontium Dating of Hydrocarbon Charge Using Small Authigenic Illitic Clay Aliquots from the Silurian Bituminous Sandstone in the Tarim Basin, NW China: Scientific Reports, v. 9, no. 1, p. 1-13.

Mackenzie, F. T., and Kump, L. R., 1995, Reverse weathering, clay mineral formation, and oceanic element cycles: Science, v. 270, no. 5236, p. 586-586.

Mählmann, R. F., Bozkaya, Ö., Potel, S., Le Bayon, R., Šegvić, B., and Nieto, F., 2012, The pioneer work of Bernard Kübler and Martin Frey in very low-grade metamorphic terranes: paleo-geothermal potential of variation in Kübler-Index/organic matter reflectance correlations. A review: Swiss Journal of Geosciences, v. 105, no. 2, p. 121-152.

McMahon, W. J., and Davies, N. S., 2018, Evolution of alluvial mudrock forced by early land plants: Science, v. 359, no. 6379, p. 1022-1024.

Mergelov, N., Mueller, C. W., Prater, I., Shorkunov, I., Dolgikh, A., Zazovskaya, E., Shishkov, V., Krupskaya, V., Abrosimov, K., and Cherkinsky, A., 2018, Alteration of rocks by endolithic organisms is one of the pathways for the beginning of soils on Earth: Scientific reports, v. 8, no. 1, p. 1-15.

Meunier, A., Velde, B., and Velde, B., 2004, Illite: Origins, evolution and metamorphism, Springer Science & Business Media.

Minster, J. F., Ricard, L. P., and Alle`gre, C. J., 1979, 87Rb-87Sr chronology of enstatite meteorites: Earth and Planetary Science Letters, v. 44, no. 3, p. 420-440.

Mukherjee, I., and Large, R. R., 2016, Pyrite trace element chemistry of the Velkerri Formation, Roper Group, McArthur Basin: Evidence for atmospheric oxygenation during the Boring Billion: Precambrian Research, v. 281, p. 13-26.

Munson, T., 2016, Sedimentary Characterisation of the Wilton Package, Greater MacArthur Basin, Northern Territory, Northern Territory Geological Survey.

Munson, T., and Revie, D., 2018, Munson TJ and Revie D, 2018. Stratigraphic subdivision of the Velkerri Formation, Roper Group, McArthur Basin, Northern Territory. Northern Territory Geological Survey, Record 2018-006.

Nebel, O., 2014, Rb–Sr Dating, Encyclopedia of Scientific Dating Methods, p. 1-19.

Nebel, O., Scherer, E. E., and Mezger, K., 2011, Evaluation of the 87Rb decay constant by age comparison against the U–Pb system: Earth and Planetary Science Letters, v. 301, no. 1, p. 1-8.

Nguyen, K., Love, G. D., Zumberge, J. A., Kelly, A. E., Owens, J. D., Rohrssen, M. K., Bates, S. M., Cai, C., and Lyons, T. W., 2019, Absence of biomarker evidence for early eukaryotic life from the Mesoproterozoic Roper Group: Searching across a marine redox gradient in mid-Proterozoic habitability: Geobiology, v. 17, no. 3, p. 247-260.

Nixon, A. L., Glorie, S., Collins, A. S., Blades, M. L., Simpson, A., and Whelan, J. A., 2021, Inter-cratonic geochronological and geochemical correlations of the Derim Derim–Galiwinku/Yanliao reconstructed Large Igneous Province across the North Australian and North China cratons: Gondwana Research.

Nixon, A. L., Glorie, S., Hasterok, D., Collins, A. S., Fernie, N., and Fraser, G., 2022, Low-temperature thermal history of the McArthur Basin: Influence of the Cambrian Kalkarindji Large Igneous Province on hydrocarbon maturation: Basin Research, v. n/a, no. n/a.

Norris, A., and Danyushevsky, L., 2018, Towards Estimating the Complete Uncertainty Budget of Quantified Results Measured by LA-ICP-MS: Goldschmidt: Boston, MA, USA.

NTGS, 1989, Altree 1 and 2 EP 24 McArthur Basin, Northern Territory Well Completion Report, Pacific Oil and Gas.

NTGS, 2009, Core Sample Analysis. Total Organic Carbon, Programmed Pyrolysis Data. Altree 2, Balmain 1, Elliott 1, Jamison 1, Core Sampling Reports: Northern Territory, Australia, Falcon Oil & Gas, Weatherford Laboratories

NTGS, 2010, EP24 Altree 2 Petrology and organic geochemistry: Eni Australia, Geotechnical Services, Falcon Oil & Gas, Northern Territory Geological Survey, CSR0185.

NTGS, 2012, Quantitative X-Ray Diffraction Analysis of 30 samples, *in* Survey, N. T. G., ed.: Northern Territory, Australia, Northern Territory Geological Survey.

NTGS, 2014, Basic Well Completion Report, NT EP167, Tarlee S3: Pangaea Resources, PR2015-0016.

NTGS, 2015, Basic Well Completion Report NT EP167 Birdum Creek 1: Pangaea Resources, PR2016-W006.

NTGS, 2016, Basic Well Completion Report NT - EP167 Wyworrie 1: Pangaea Resources, PR2016-W007.

Ola, P. S., Aidi, A. K., and Bankole, O. M., 2018, Clay mineral diagenesis and source rock assessment in the Bornu Basin, Nigeria: Implications for thermal maturity and source rock potential: Marine and Petroleum Geology, v. 89, p. 653-664.

Olierook, H. K., Rankenburg, K., Ulrich, S., Kirkland, C. L., Evans, N. J., Brown, S., McInnes, B. I., Prent, A., Gillespie, J., and McDonald, B., 2020, Resolving multiple geological events using in situ Rb–Sr geochronology: implications for metallogenesis at Tropicana, Western Australia: Geochronology, v. 2, no. 2, p. 283-303.

Page, R. W., Jackson, M. J., and Krassay, A. A., 2000, Constraining sequence stratigraphy in north Australian basins: SHRIMP U–Pb zircon geochronology between Mt Isa and McArthur River*: Australian Journal of Earth Sciences, v. 47, no. 3, p. 431-459.

Papanastassiou, D. A., and Wasserburg, G. J., 1970, RbSr ages from the ocean of storms: Earth and Planetary Science Letters, v. 8, no. 4, p. 269-278.

Pearce, N. J., Perkins, W. T., Westgate, J. A., Gorton, M. P., Jackson, S. E., Neal, C. R., and Chenery, S. P., 1997, A compilation of new and published major and trace element data for NIST SRM 610 and NIST SRM 612 glass reference materials: Geostandards newsletter, v. 21, no. 1, p. 115-144.

Peters, K. E., 1986, Guidelines for evaluating petroleum source rock using programmed pyrolysis: AAPG bulletin, v. 70, no. 3, p. 318-329.

Peters, K. E., and Cassa, M. R., 1994, Applied source rock geochemistry: Chapter 5: Part II. Essential elements.

Piedad-Sánchez, N., Izart, A., Martínez, L., Suárez-Ruiz, I., Elie, M., and Menetrier, C., 2004, Paleothermicity in the Central Asturian Coal Basin, North Spain: International Journal of Coal Geology, v. 58, no. 4, p. 205-229.

Plumb, K., and Wellman, P., 1987, McArthur Basin, Northern Territory: mapping of deep troughs using gravity and magnetic anomalies: BMR Journal of Australian Geology & Geophysics, v. 10, no. 3, p. 243-251.

Poitrasson, F., Pin, C., and Duthou, J.-L., 1995, Hydrothermal remobilization of rare earth elements and its effect on Nd isotopes in rhyolite and granite: Earth and Planetary Science Letters, v. 130, no. 1, p. 1-11.

Pollastro, R. M., 1993, Considerations and applications of the illite/smectite geothermometer in hydrocarbon-bearing rocks of Miocene to Mississippian age: Clays and Clay minerals, v. 41, p. 119-119.

Radke, M., Willsch, H., Leythaeuser, D., and Teichmüller, M., 1982, Aromatic components of coal: relation of distribution pattern to rank: Geochimica et Cosmochimica Acta, v. 46, no. 10, p. 1831-1848.

Rafiei, M., and Kennedy, M., 2019, Weathering in a world without terrestrial life recorded in the Mesoproterozoic Velkerri Formation: Nature Communications, v. 10, no. 1, p. 3448.

Rafiei, M., Löhr, S., Baldermann, A., Webster, R., and Kong, C., 2020, Quantitative petrographic differentiation of detrital vs diagenetic clay minerals in marine sedimentary sequences: Implications for the rise of biotic soils: Precambrian Research, v. 350, p. 105948.

Rawlings, D. J., 1999, Stratigraphic resolution of a multiphase intracratonic basin system: the McArthur Basin, northern Australia: Australian Journal of Earth Sciences, v. 46, no. 5, p. 703-723.

Redaa, A., Farkaš, J., Gilbert, S., Collins, A. S., Wade, B., Löhr, S., Zack, T., and Garbe-Schönberg, D., 2021a, Assessment of elemental fractionation and matrix effects during in situ Rb–Sr dating of phlogopite by LA-ICP-MS/MS: implications for the accuracy and precision of mineral ages: Journal of Analytical Atomic Spectrometry.

Redaa, A., Farkaš, J., Hassan, A., Collins, A. S., Gilbert, S., and Löhr, S. C., 2021b, Constraints from in-situ Rb-Sr dating on the timing of tectono-thermal events in the Umm Farwah shear zone and associated Cu-Au mineralisation in the Southern Arabian Shield, Saudi Arabia: Journal of Asian Earth Sciences, p. 105037.

Revie, D., 2014, XRD analysis greater McArthur Basin, *in* Survey, N. T. G., ed.: Northern Territory, Australia, Northern Territory Geological Survey.

Revie, D., 2016, Interpretive summary of integrated petroleum geochemistry of selected wells in the greater McArthur Basin, NT, Australia: Northern Territory Geological Survey, Weatherford Laboratories, CSR0413.

Revie, D., and MacDonald, G., Volumetric resource assessment of the lower Kyalla and middle Velkerri formations of the McArthur Basin, *in* Proceedings Annual Geoscience Exploration Seminar (AGES) Proceedings2017, Volume 28, p. 29.

Revie, D., Normington, V., and Jarrett, A., 2022, Shale resource data from the greater McArthur Basin: Northern Territory Geological Survey, 1445-5358.

Ribeiro, B. V., Finch, M. A., Cawood, P. A., Faleiros, F. M., Murphy, T. D., Simpson, A., Glorie, S., Tedeschi, M., Armit, R., and Barrote, V. R., 2021, From microanalysis to supercontinents: Insights from the Rio Apa Terrane into the Mesoproterozoic SW Amazonian Craton evolution during Rodinia assembly: Journal of Metamorphic Geology, v. n/a, no. n/a.

Riediger, C. L., 1993, Solid bitumen reflectance and Rock-Eval Tmax as maturation indices: an example from the "Nordegg Member", Western Canada Sedimentary Basin: International Journal of Coal Geology, v. 22, no. 3, p. 295-315.

Rösel, D., and Zack, T., 2022, LA-ICP-MS/MS Single-Spot Rb-Sr Dating: Geostandards and Geoanalytical Research, v. 46, no. 2, p. 143-168.

Sander, R., Pan, Z., Connell, L. D., Camilleri, M., Grigore, M., and Yang, Y., 2018, Controls on methane sorption capacity of Mesoproterozoic gas shales from the Beetaloo Sub-basin, Australia and global shales: International Journal of Coal Geology, v. 199, p. 65-90.

Scheiblhofer, E., Moser, U., Löhr, S., Wilmsen, M., Farkaš, J., Gallhofer, D., Bäckström, A. M., Zack, T., and Baldermann, A., 2022, Revisiting Glauconite Geochronology: Lessons Learned from In Situ Radiometric Dating of a Glauconite-Rich Cretaceous Shelfal Sequence: Minerals, v. 12, no. 7, p. 818.

Schmitz, M. D., and Schoene, B., 2007, Derivation of isotope ratios, errors, and error correlations for U-Pb geochronology using 205Pb-235U-(233U)-spiked isotope dilution thermal ionization mass spectrometric data: Geochemistry, Geophysics, Geosystems, v. 8, no. 8.

Selby, D., 2009, U-Pb zircon geochronology of the Aptian/Albian boundary implies that the GL-O international glauconite standard is anomalously young: Cretaceous Research, v. 30, no. 5, p. 1263-1267.

Şengün, F., Bertrandsson Erlandsson, V., Hogmalm, J., and Zack, T., 2019, In situ Rb-Sr dating of K-bearing minerals from the orogenic Akçaabat gold deposit in the Menderes Massif, Western Anatolia, Turkey: Journal of Asian Earth Sciences, v. 185, p. 104048.

Shepherd, T. J., and Darbyshire, D. P. F., 1981, Fluid inclusion Rb–Sr isochrons for dating mineral deposits: Nature, v. 290, no. 5807, p. 578-579.

Simmons, E. C., 1998, rubidiumRubidium: Element and geochemistry, Geochemistry: Dordrecht, Springer Netherlands, p. 555-556.

Simpson, A., Gilbert, S., Tamblyn, R., Hand, M., Spandler, C., Gillespie, J., Nixon, A., and Glorie, S., 2021, In-situ LuHf geochronology of garnet, apatite and xenotime by LA ICP MS/MS: Chemical Geology, v. 577, p. 120299.

Simpson, A., Glorie, S., Hand, M., Spandler, C., Gilbert, S., and Cave, B., 2022, In situ Lu–Hf geochronology of calcite: Geochronology, v. 4, no. 1, p. 353-372.

Singer, A., 1980, The paleoclimatic interpretation of clay minerals in soils and weathering profiles: Earth-Science Reviews, v. 15, no. 4, p. 303-326.

Southgate, P. N., Bradshaw, B. E., Domagala, J., Jackson, M. J., Idnurm, M., Krassay, A. A., Page, R. W., Sami, T. T., Scott, D. L., Lindsay, J. F., McConachie, B. A., and Tarlowski, C., 2000, Chronostratigraphic basin framework for Palaeoproterozoic rocks (1730–1575 Ma) in northern Australia and implications for base-metal mineralisation: Australian Journal of Earth Sciences, v. 47, no. 3, p. 461-483.

Subarkah, D., Blades, M. L., Collins, A. S., Farkaš, J., Gilbert, S., Löhr, S. C., Redaa, A., Cassidy, E., and Zack, T., 2021, Unraveling the histories of Proterozoic shales through in situ Rb-Sr dating and trace element laser ablation analysis: Geology.

Summons, R. E., Taylor, D., and Boreham, C. J., 1994, Geochemical Tools For Evaluating Petroleum Generation In Middle Proterozoic Sediments Of The Mcarthur Basin, Northern Territory, Australia: The APPEA Journal, v. 34, no. 1, p. 692-706.

Tamblyn, R., Hand, M., Morrissey, L., Zack, T., Phillips, G., and Och, D., 2020, Resubduction of lawsonite eclogite within a serpentinite-filled subduction channel: Contributions to Mineralogy and Petrology, v. 175, no. 8, p. 74.

Tamblyn, R., Hand, M., Simpson, A., Gilbert, S., Wade, B., and Glorie, S., 2021, In situ laser ablation Lu–Hf geochronology of garnet across the Western Gneiss Region: campaign-style dating of metamorphism: Journal of the Geological Society.

Taylor, D., Kontorovich, A. E., Larichev, A. I., and Glikson, M., 1994, Petroleum Source Rocks In The Roper Group Of The Mcarthur Basin: Source Characterisation And Maturity Determinations Using Physical And Chemical Methods: The APPEA Journal, v. 34, no. 1, p. 279-296.

Tillberg, M., Drake, H., Zack, T., Kooijman, E., Whitehouse, M. J., and Åström, M. E., 2020, In situ Rb-Sr dating of slickenfibres in deep crystalline basement faults: Scientific Reports, v. 10, no. 1, p. 562.

Tissot, B., Durand, B., Espitalie, J., and Combaz, A., 1974, Influence of nature and diagenesis of organic matter in formation of petroleum: Aapg Bulletin, v. 58, no. 3, p. 499-506.

Tissot, B., Pelet, R., and Ungerer, P., 1987, Thermal history of sedimentary basins, maturation indices, and kinetics of oil and gas generation: AAPG bulletin, v. 71, no. 12, p. 1445-1466.

Torgersen, E., Viola, G., Zwingmann, H., and Harris, C., 2015, Structural and temporal evolution of a reactivated brittle–ductile fault – Part II: Timing of fault initiation and reactivation by K–Ar dating of synkinematic illite/muscovite: Earth and Planetary Science Letters, v. 410, p. 212-224.

Varajao, A., and Meunier, A., 1995, Particle morphological evolution during the conversion of I/S to illite in Lower Cretaceous shales from Sergipe-Alagoas Basin, Brazil: Clays and Clay minerals, v. 43, no. 1, p. 14-28.

Velde, B., and Espitalié, J., 1989, Comparison of kerogen maturation and illite/smectite somposition in diagnesis: Journal of Petroleum Geology, v. 12, no. 1, p. 103-110.

Velde, B., and Vasseur, G., 1992, Estimation of the diagenetic smectite to illite transformation in time-temperature space: American Mineralogist, v. 77, no. 9-10, p. 967-976.

Vermeesch, P., 2007, Quantitative geomorphology of the White Mountains (California) using detrital apatite fission track thermochronology: Journal of Geophysical Research: Earth Surface, v. 112, no. F3.

Vermeesch, 2012, On the visualisation of detrital age distributions: Chemical Geology, v. 312-313, p. 190-194.

Vermeesch, 2013, Multi-sample comparison of detrital age distributions: Chemical Geology, v. 341, p. 140-146.

Vermeesch, 2018, IsoplotR : A free and open toolbox for geochronology: Geoscience Frontiers, v. 9.

Villa, 1998, Isotopic closure: Terra Nova, v. 10, no. 1, p. 42-47.

Villa, I. M., De Bièvre, P., Holden, N., and Renne, P., 2015, IUPAC-IUGS recommendation on the half life of 87Rb: Geochimica et Cosmochimica Acta, v. 164, p. 382-385.

Volk, H., George, S. C., Dutkiewicz, A., and Ridley, J., 2005, Characterisation of fluid inclusion oil in a Mid-Proterozoic sandstone and dolerite (Roper Superbasin, Australia): Chemical Geology, v. 223, no. 1, p. 109-135.

Waliczek, M., Machowski, G., Poprawa, P., Świerczewska, A., and Więcław, D., 2021, A novel VRo, Tmax, and S indices conversion formulae on data from the fold-and-thrust belt of

the Western Outer Carpathians (Poland): International Journal of Coal Geology, v. 234, p. 103672.
Wang, X.-C., Li, Z.-X., Li, X.-H., Li, J., Liu, Y., Long, W.-G., Zhou, J.-B., and Wang, F. J. J. o. P., 2012, Temperature, pressure, and composition of the mantle source region of Late Cenozoic basalts in Hainan Island, SE Asia: a consequence of a young thermal mantle plume close to subduction zones?, v. 53, no. 1, p. 177-233.
Waples, D. W., 1980, Time and temperature in petroleum formation: application of Lopatin's method to petroleum exploration: AAPG bulletin, v. 64, no. 6, p. 916-926.
Warr, L., and Mählmann, R. F., 2015, Recommendations for Kübler index standardization: Clay Minerals, v. 50, no. 3, p. 283-286.
Warr, L., and Rice, A. J. J. o. m. G., 1994, Interlaboratory standardization and calibration of day mineral crystallinity and crystallite size data, v. 12, no. 2, p. 141-152.
Warren, J. K., George, S. C., Hamilton, P. J., and Tingate, P., 1998, Proterozoic Source Rocks: Sedimentology and Organic Characteristics of the Velkerri Formation, Northern Territory, Australia1: AAPG Bulletin, v. 82, no. 3, p. 442-463.
Welte, D., and Tissot, P., 1984, Petroleum formation and occurrence, Springer.
Wilhelms, A., Telnæs, N., Steen, A., and Augustson, J., 1998, A quantitative study of aromatic hydrocarbons in a natural maturity shale sequence—the 3-methylphenanthrene/retene ratio, a pragmatic maturity parameter: Organic Geochemistry, v. 29, no. 1, p. 97-105.
Williams-Jones, A., Migdisov, A., and Samson, I., 2012, Hydrothermal Mobilisation of the Rare Earth Elements - a Tale of "Ceria" and "Yttria": Elements, v. 8, p. 355-360.
Wilson, M. J., 1999, The origin and formation of clay minerals in soils: past, present and future perspectives: Clay minerals, v. 34, no. 1, p. 7-25.
Yang, B., Collins, A., Blades, M., Capogreco, N., Payne, J., Munson, T., Cox, G., and Glorie, S., 2019, Middle-late Mesoproterozoic tectonic geography of the North Australia Craton: U–Pb and Hf isotopes of detrital zircon grains in the Beetaloo Sub-basin, Northern Territory, Australia: Journal of the Geological Society, v. 176, p. jgs2018-2159.
Yang, B., Collins, A. S., Cox, G. M., Jarrett, A. J. M., Denyszyn, S., Blades, M. L., Farkaš, J., and Glorie, S., 2020, Using Mesoproterozoic Sedimentary Geochemistry to Reconstruct Basin Tectonic Geography and Link Organic Carbon Productivity to Nutrient Flux from a Northern Australian Large Igneous Province: Basin Research, v. n/a, no. n/a.
Yang, B., Smith, T. M., Collins, A. S., Munson, T. J., Schoemaker, B., Nicholls, D., Cox, G., Farkas, J., and Glorie, S., 2018, Spatial and temporal variation in detrital zircon age provenance of the hydrocarbon-bearing upper Roper Group, Beetaloo Sub-basin, Northern Territory, Australia: Precambrian Research, v. 304, p. 140-155.
Yang, S., and Horsfield, B., 2020, Critical review of the uncertainty of Tmax in revealing the thermal maturity of organic matter in sedimentary rocks: International Journal of Coal Geology, v. 225, p. 103500.
Yang, Y.-h., Zhang, H.-f., Chu, Z.-y., Xie, L.-w., and Wu, F.-y., 2010, Combined chemical separation of Lu, Hf, Rb, Sr, Sm and Nd from a single rock digest and precise and accurate isotope determinations of Lu–Hf, Rb–Sr and Sm–Nd isotope systems using Multi-Collector ICP-MS and TIMS: International Journal of Mass Spectrometry, v. 290, no. 2-3, p. 120-126.
Yim, S.-G., Jung, M.-J., Jeong, Y.-J., Kim, Y., and Cheong, A. C.-s., 2021, Mass fractionation of Rb and Sr isotopes during laser ablation-multicollector-ICPMS: in situ observation and correction: Journal of Analytical Science and Technology, v. 12, no. 1, p. 10.

Yoder, H. S., and Eugster, H. P., 1955, Synthetic and natural muscovites: Geochimica et Cosmochimica Acta, v. 8, no. 5, p. 225-280.

Zack, T., and Hogmalm, K. J., 2016, Laser ablation Rb/Sr dating by online chemical separation of Rb and Sr in an oxygen-filled reaction cell: Chemical Geology, v. 437, p. 120-133.

Zambell, C., Adams, J., Gorring, M., and Schwartzman, D., 2012, Effect of lichen colonization on chemical weathering of hornblende granite as estimated by aqueous elemental flux: Chemical Geology, v. 291, p. 166-174.

A.

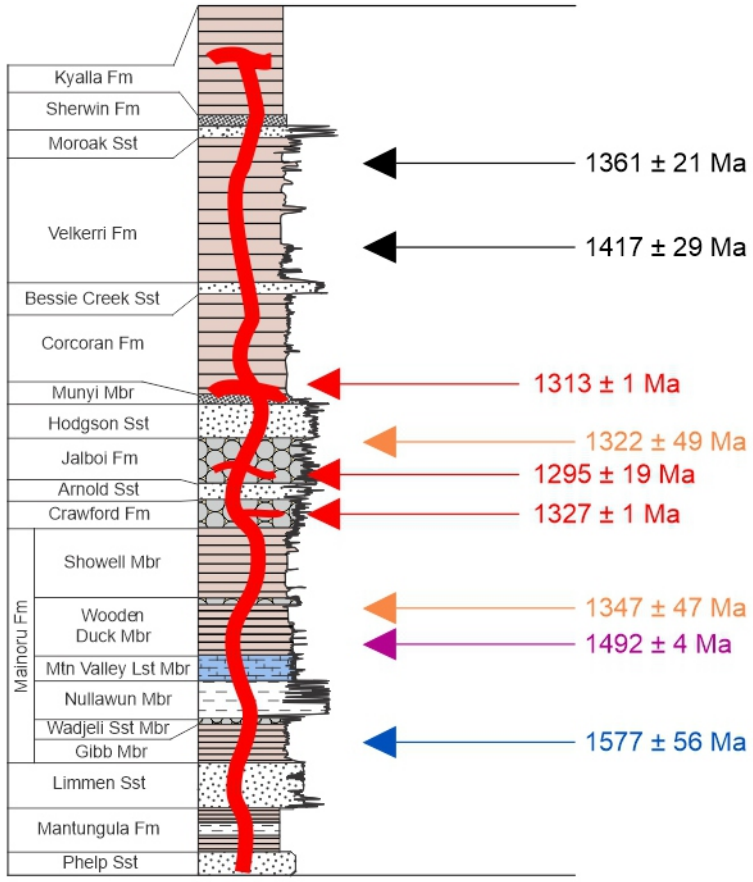
Kyalla Fm
Sherwin Fm
Moroak Sst
Velkerri Fm
Bessie Creek Sst
Corcoran Fm
Munyi Mbr
Hodgson Sst
Jalboi Fm
Arnold Sst
Crawford Fm
Showell Mbr
Wooden Duck Mbr
Mtn Valley Lst Mbr
Nullawun Mbr
Wadjeli Sst Mbr
Gibb Mbr
Limmen Sst
Mainoru Fm
Mantungula Fm
Phelp Sst
1361 ± 21 Ma
1417 ± 29 Ma
1313 ± 1 Ma
1322 ± 49 Ma
1295 ± 19 Ma
1327 ± 1 Ma
1347 ± 47 Ma
1492 ± 4 Ma
1577 ± 56 Ma

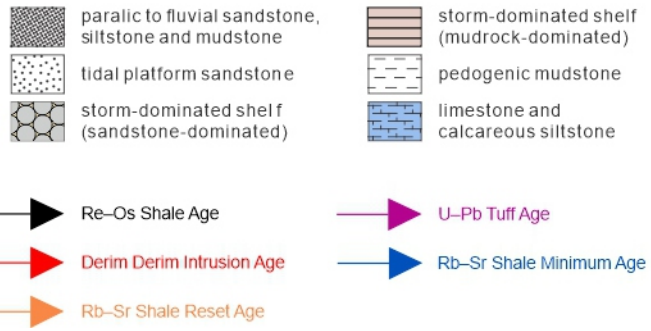
paralic to fluvial sandstone, siltstone and mudstone
tidal platform sandstone
storm-dominated shelf (sandstone-dominated)
storm-dominated shelf (mudrock-dominated)
pedogenic mudstone
limestone and calcareous siltstone

Re–Os Shale Age
Derim Derim Intrusion Age
Rb–Sr Shale Reset Age
U–Pb Tuff Age
Rb–Sr Shale Minimum Age

B.

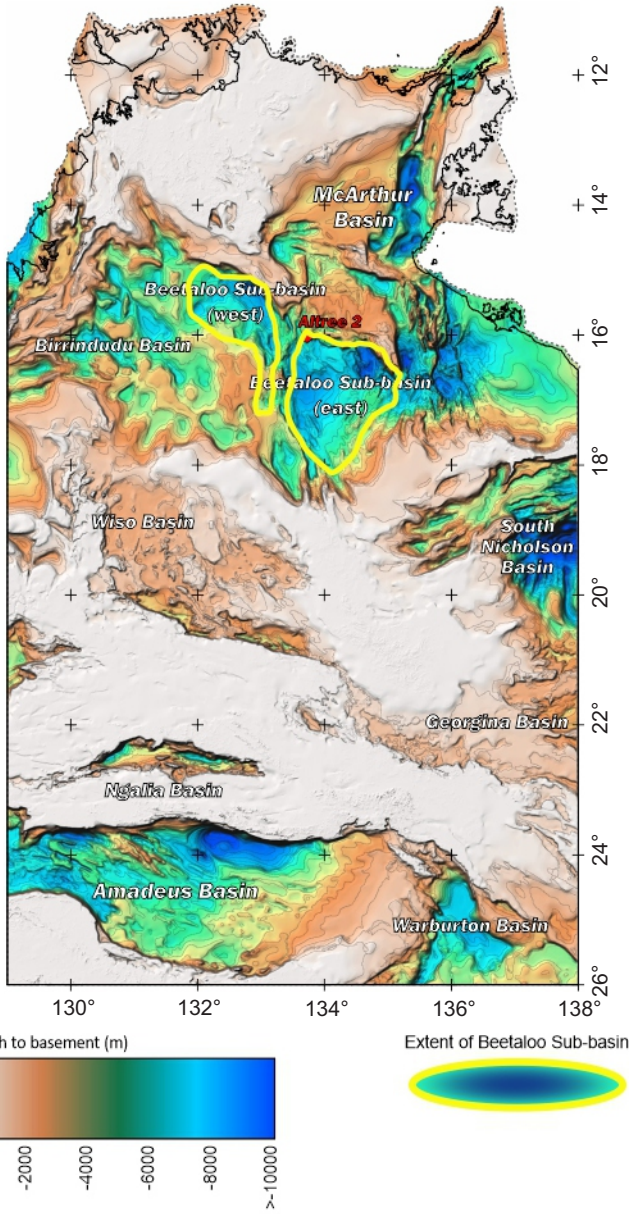
McArthur Basin
Beetaloo Sub-basin (west)
Altree 2
Birrindudu Basin
Beetaloo Sub-basin (east)
Wiso Basin
South Nicholson Basin
Georgina Basin
Ngalia Basin
Amadeus Basin
Warburton Basin
12°
14°
16°
18°
20°
22°
24°
26°
130°
132°
134°
136°
138°
Depth to basement (m)
0
-2000
-4000
-6000
-8000
>-10000
Extent of Beetaloo Sub-basin

Figure 1

Figure 2

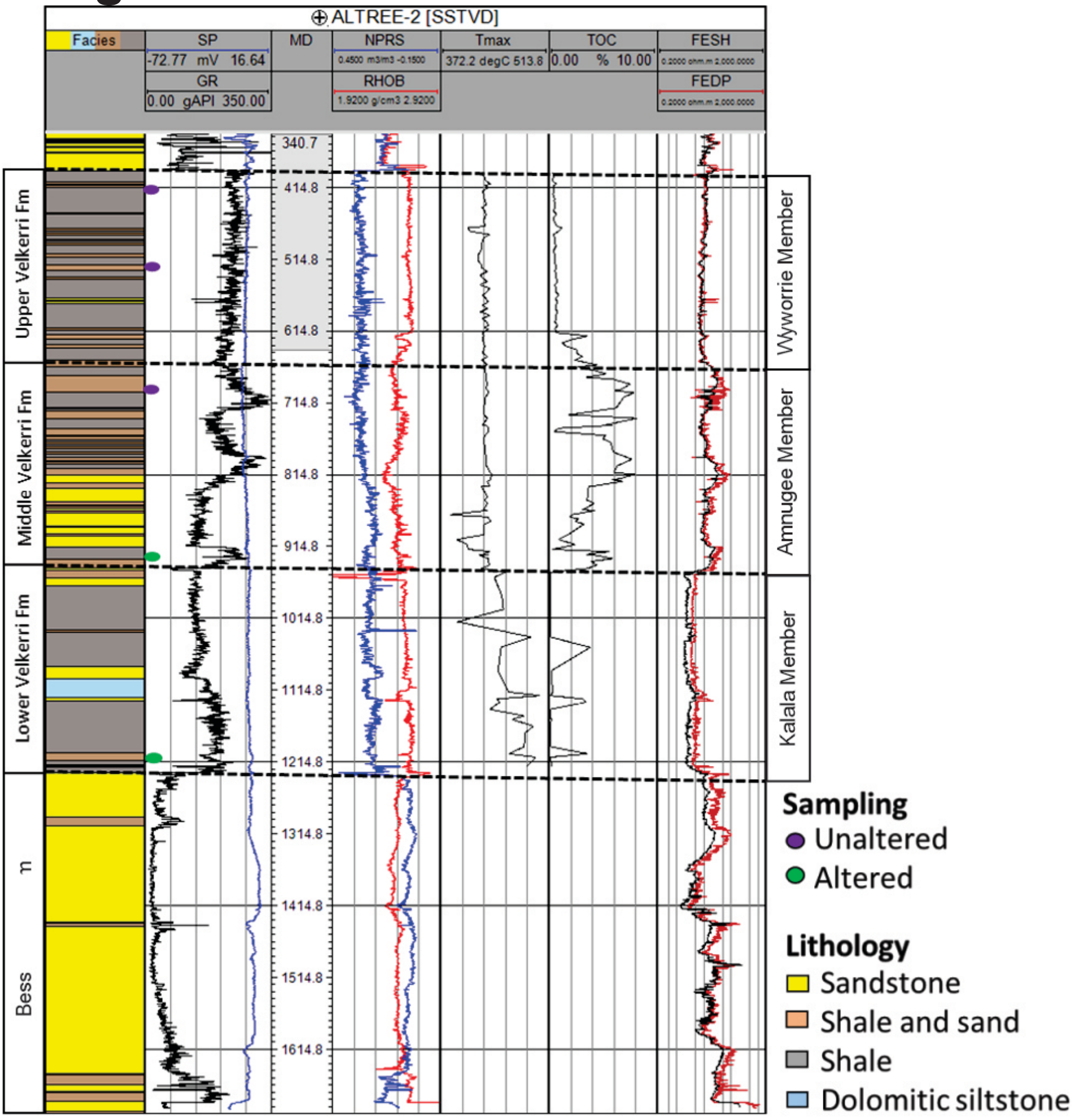
ALTREE-2 [SSTVD]
Facies
SP
-72.77 mV 16.64
GR
0.00 gAPI 350.00
MD
NPRS
0.4500 m3/m3 -0.1500
RHOB
1.9200 g/cm3 2.9200
Tmax
372.2 degC 513.8
TOC
0.00 % 10.00
FESH
0.2000 ohm.m 2,000.0000
FEDP
0.2000 ohm.m 2,000.0000
340.7
414.8
514.8
614.8
714.8
814.8
914.8
1014.8
1114.8
1214.8
1314.8
1414.8
1514.8
1614.8
Upper Velkerri Fm
Middle Velkerri Fm
Lower Velkerri Fm
Bessηη
Wyworrie Member
Amnugee Member
Kalala Member
Sampling
Unaltered
Altered
Lithology
Sandstone
Shale and sand
Shale
Dolomitic siltstone

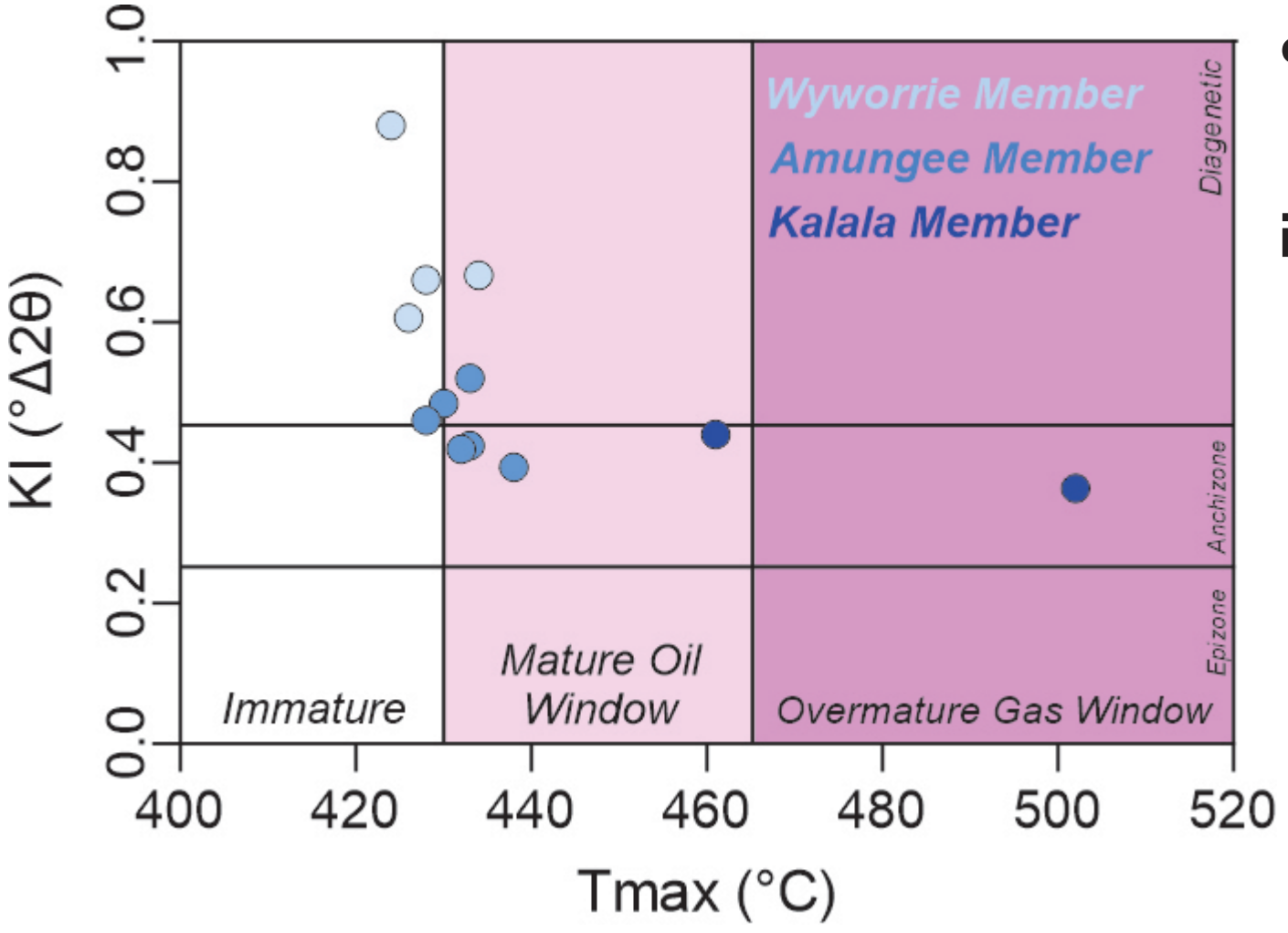
KI (°Δ2θ)
1.0
0.8
0.6
0.4
0.2
0.0
400
420
440
460
480
500
520
Tmax (°C)
Wyworrie Member
Amungee Member
Kalala Member
Diagenetic
Anchizone
Epizone
Immature
Mature Oil Window
Overmature Gas Window

Figure 3

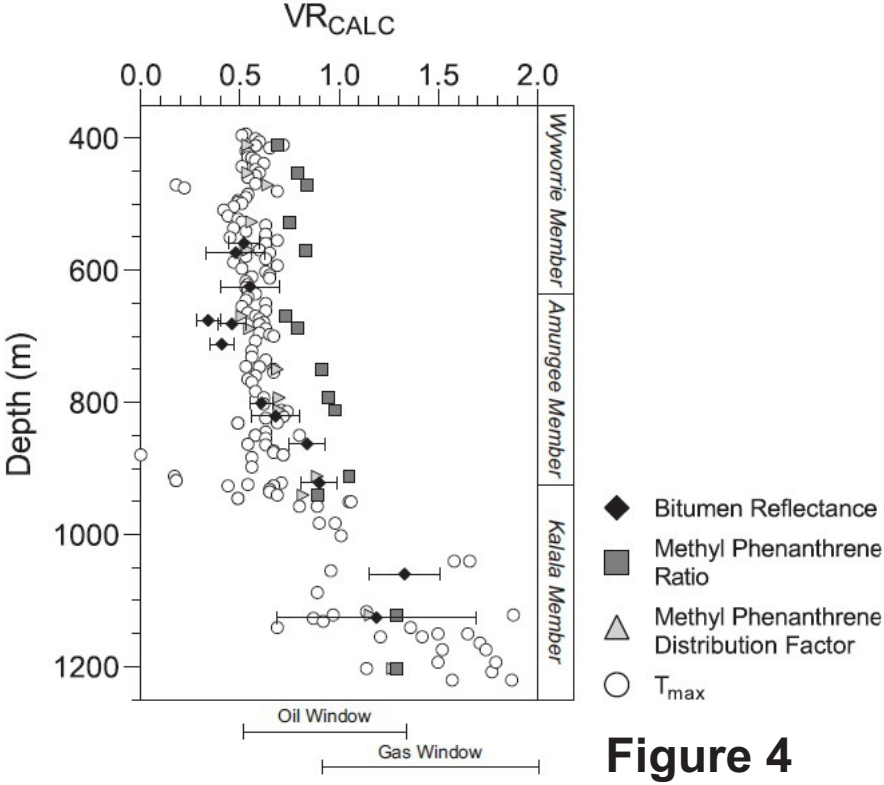
VRCALC
0.0
0.5
1.0
1.5
2.0
400
600
800
1000
1200
Depth (m)
Wyworrie Member
Amungee Member
Kalala Member
Oil Window
Gas Window
Bitumen Reflectance
Methyl Phenanthrene Ratio
Methyl Phenanthrene Distribution Factor
Tmax

Figure 4

Figure 5

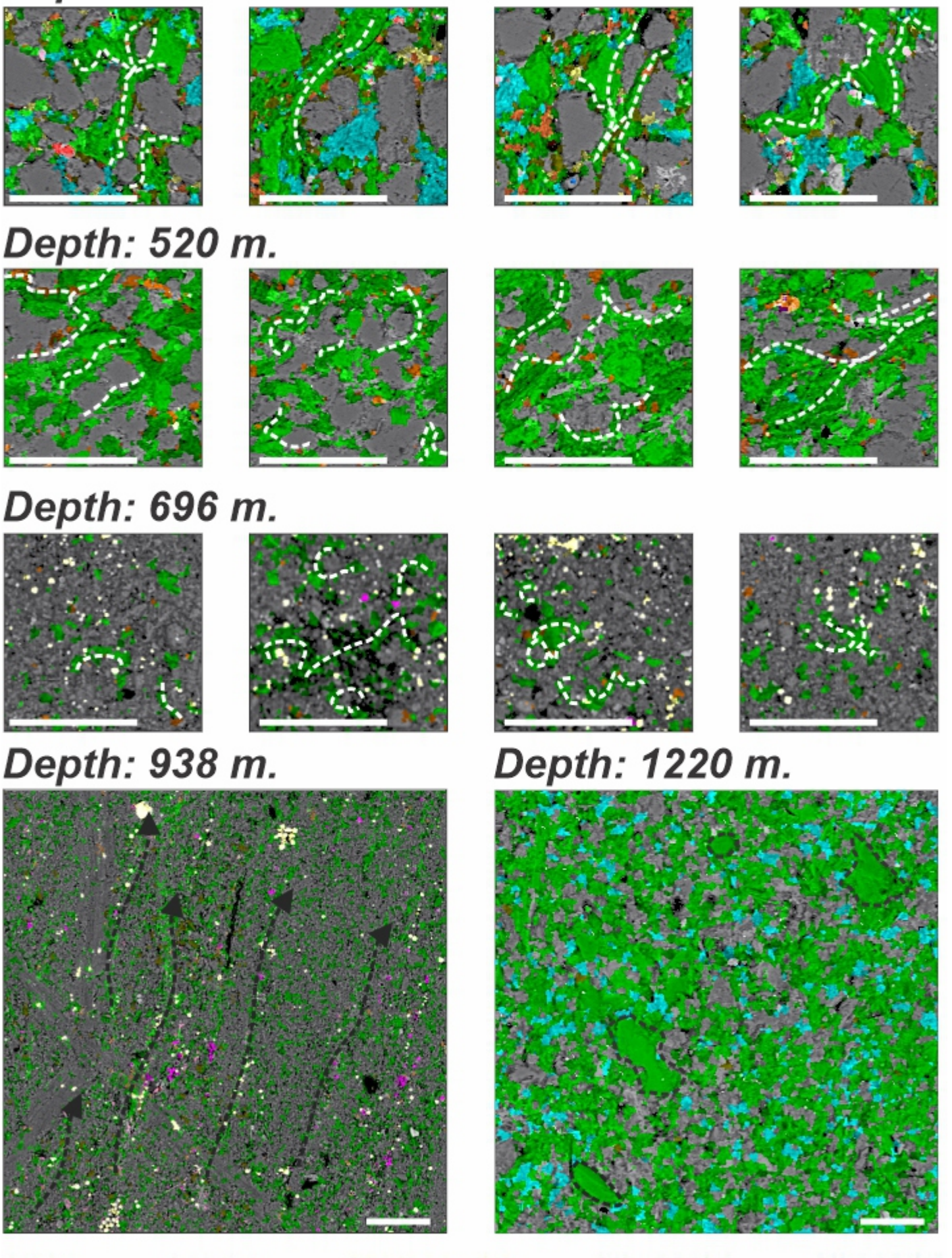
Depth: 415 m.
Depth: 520 m.
Depth: 696 m.
Depth: 938 m.
Depth: 1220 m.
Albite
Apatite
Chalcopyrite
Glauconite
Magnetite
Illite
Kaolonite
Organic Matter
Pyrite
Quartz
Zircon

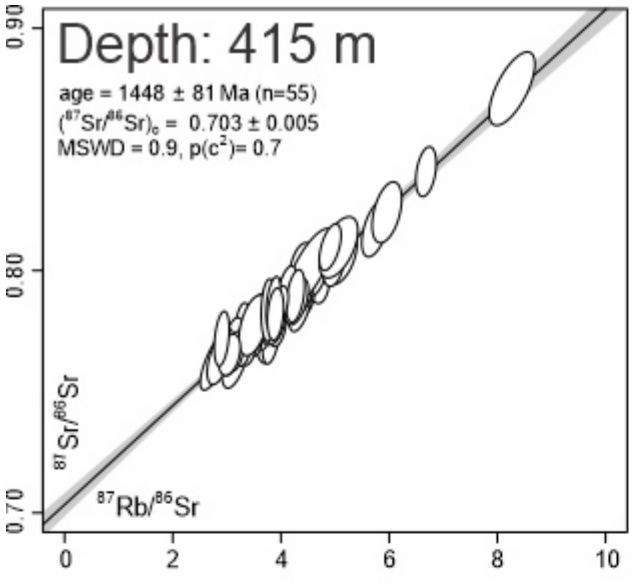
Depth: 415 m
age = 1448 ± 81 Ma (n=55)
$(^{87}Sr/^{86}Sr)_c$ = 0.703 ± 0.005
MSWD = 0.9, $p(c^2)$= 0.7
$^{87}Sr/^{86}Sr$
$^{87}Rb/^{86}Sr$
0.70
0.80
0.90
0
2
4
6
8
10

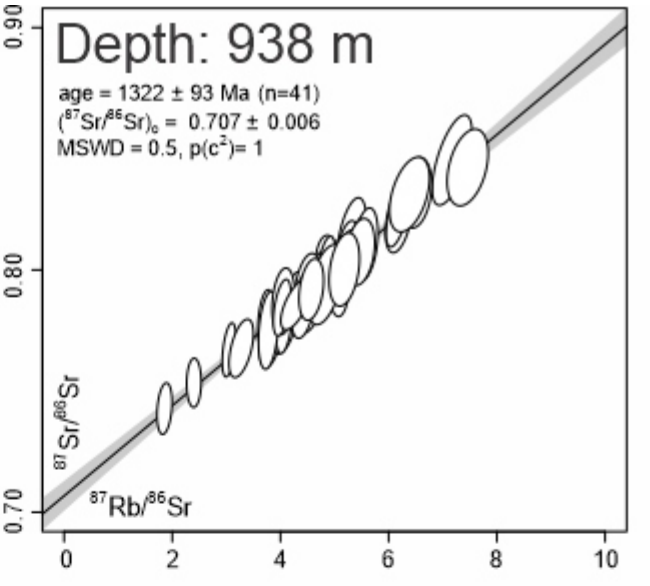
Depth: 938 m
age = 1322 ± 93 Ma (n=41)
$(^{87}Sr/^{86}Sr)_c$ = 0.707 ± 0.006
MSWD = 0.5, $p(c^2)$= 1
$^{87}Sr/^{86}Sr$
$^{87}Rb/^{86}Sr$
0.70
0.80
0.90
0
2
4
6
8
10

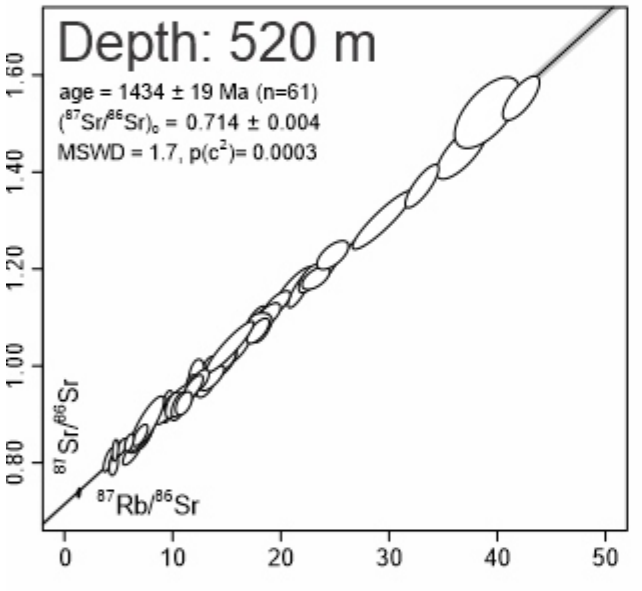
Depth: 520 m
age = 1434 ± 19 Ma (n=61)
$(^{87}Sr/^{86}Sr)_c$ = 0.714 ± 0.004
MSWD = 1.7, $p(c^2)$= 0.0003
$^{87}Sr/^{86}Sr$
$^{87}Rb/^{86}Sr$
0.80
1.00
1.20
1.40
1.60
0
10
20
30
40
50

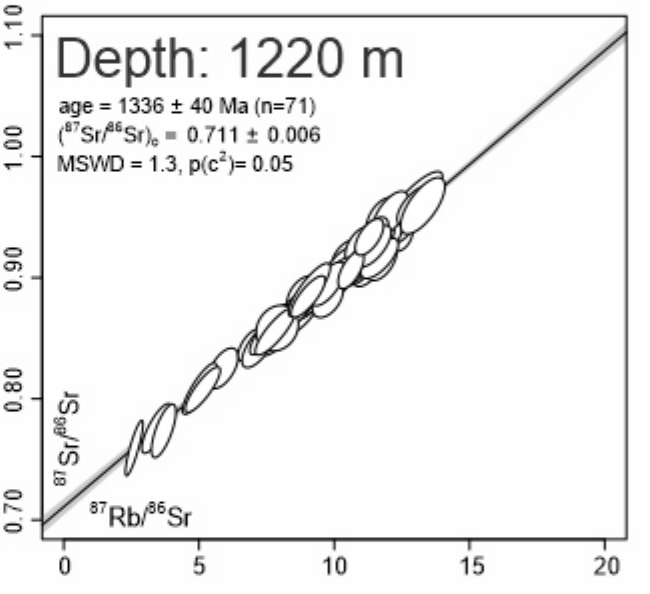
Depth: 1220 m
age = 1336 ± 40 Ma (n=71)
$(^{87}Sr/^{86}Sr)_c$ = 0.711 ± 0.006
MSWD = 1.3, $p(c^2)$= 0.05
$^{87}Sr/^{86}Sr$
$^{87}Rb/^{86}Sr$
0.70
0.80
0.90
1.00
1.10
0
5
10
15
20

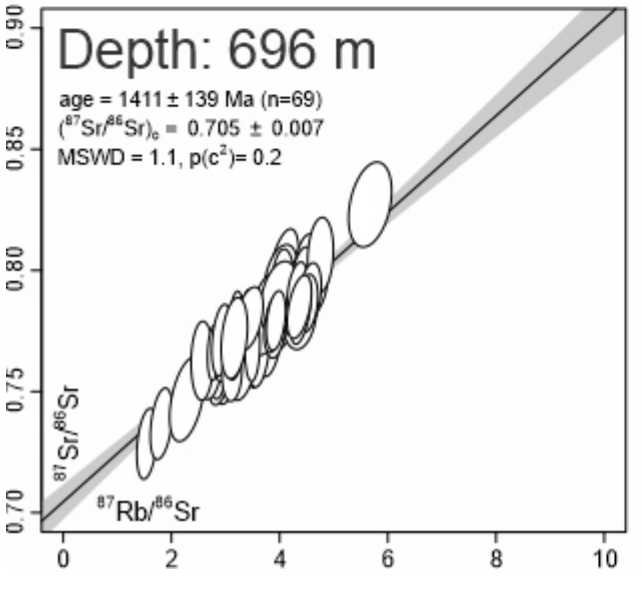
Depth: 696 m
age = 1411 ± 139 Ma (n=69)
$(^{87}Sr/^{86}Sr)_c$ = 0.705 ± 0.007
MSWD = 1.1, $p(c^2)$= 0.2
$^{87}Sr/^{86}Sr$
$^{87}Rb/^{86}Sr$
0.70
0.75
0.80
0.85
0.90
0
2
4
6
8
10

Figure 6

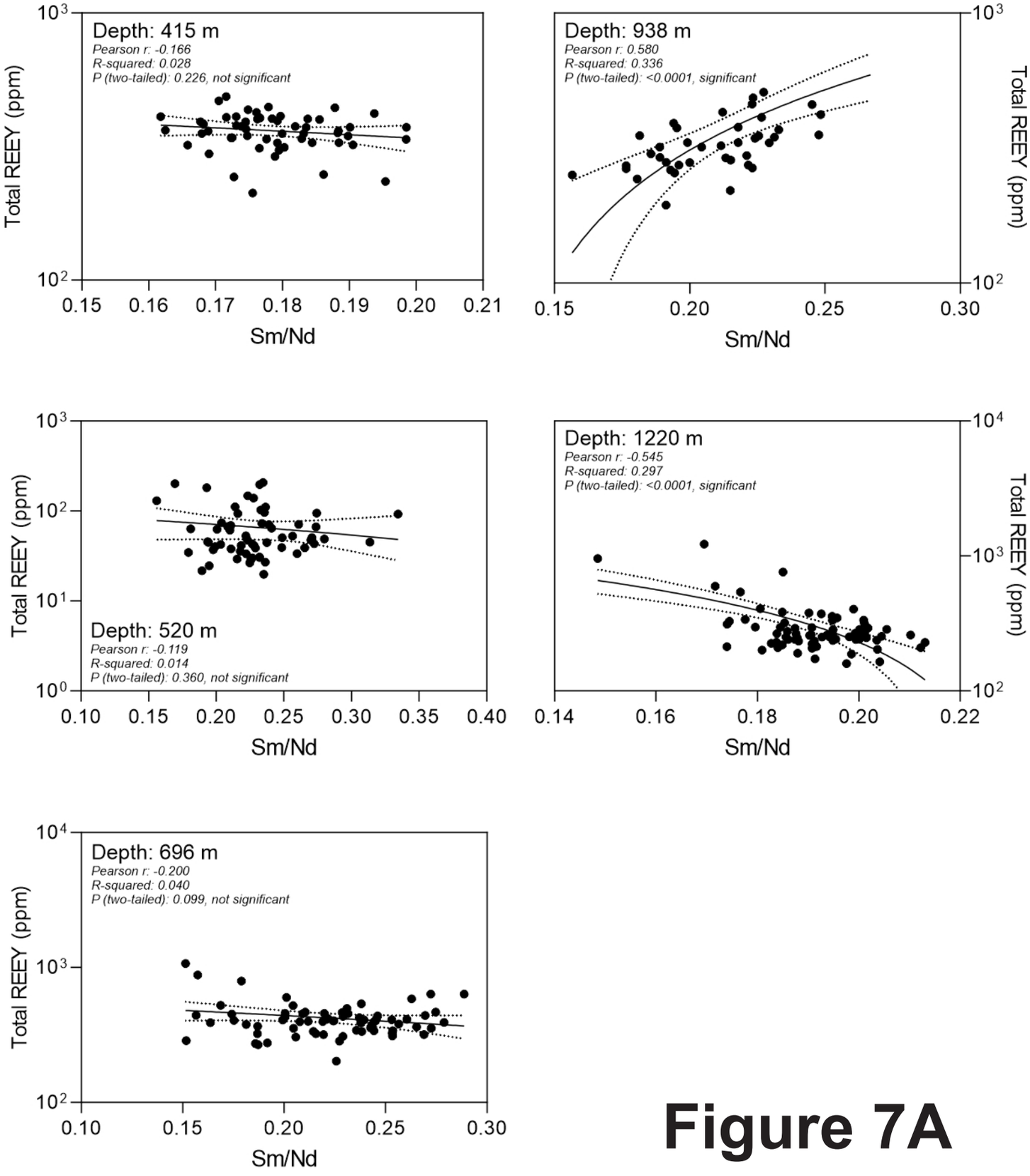
Depth: 415 m
Pearson r: -0.166
R-squared: 0.028
P (two-tailed): 0.226, not significant
Depth: 938 m
Pearson r: 0.580
R-squared: 0.336
P (two-tailed): <0.0001, significant
Depth: 520 m
Pearson r: -0.119
R-squared: 0.014
P (two-tailed): 0.360, not significant
Depth: 1220 m
Pearson r: -0.545
R-squared: 0.297
P (two-tailed): <0.0001, significant
Depth: 696 m
Pearson r: -0.200
R-squared: 0.040
P (two-tailed): 0.099, not significant
Total REEY (ppm)
Sm/Nd

Figure 7A

Figure 7B

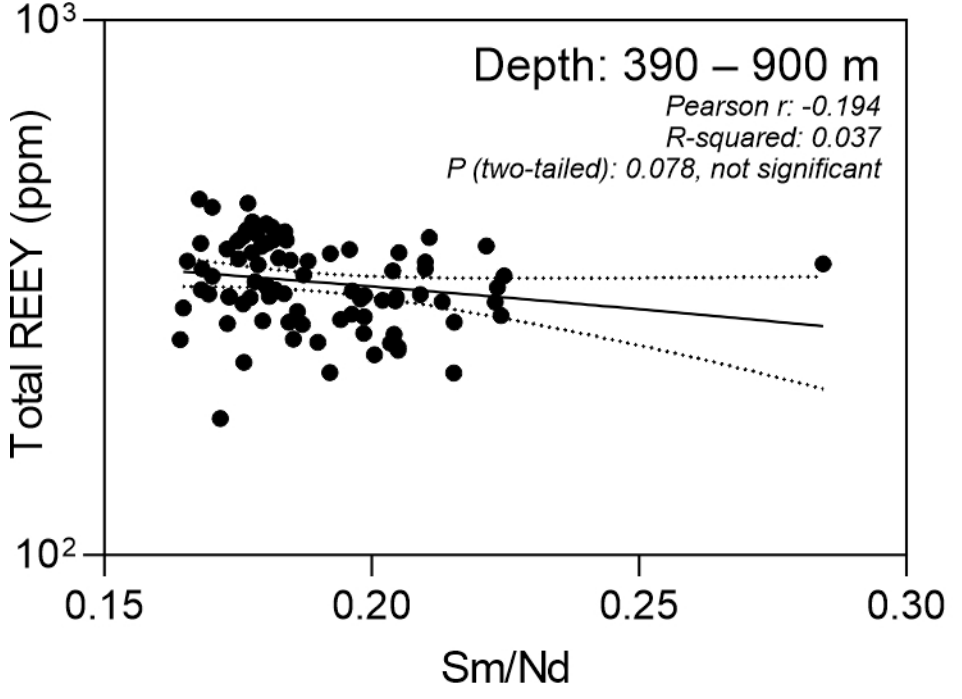
Depth: 390 – 900 m
Pearson r: -0.194
R-squared: 0.037
P (two-tailed): 0.078, not significant
Total REEY (ppm)
10³
10²
0.15
0.20
0.25
0.30
Sm/Nd

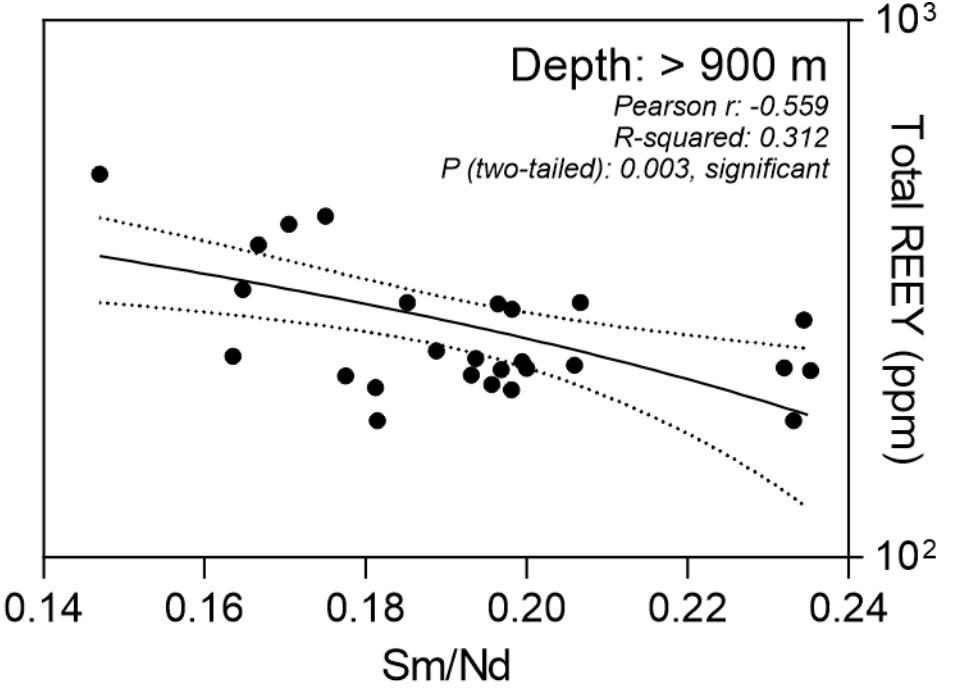
Depth: > 900 m
Pearson r: -0.559
R-squared: 0.312
P (two-tailed): 0.003, significant
Total REEY (ppm)
10³
10²
0.14
0.16
0.18
0.20
0.22
0.24
Sm/Nd

Figure 8

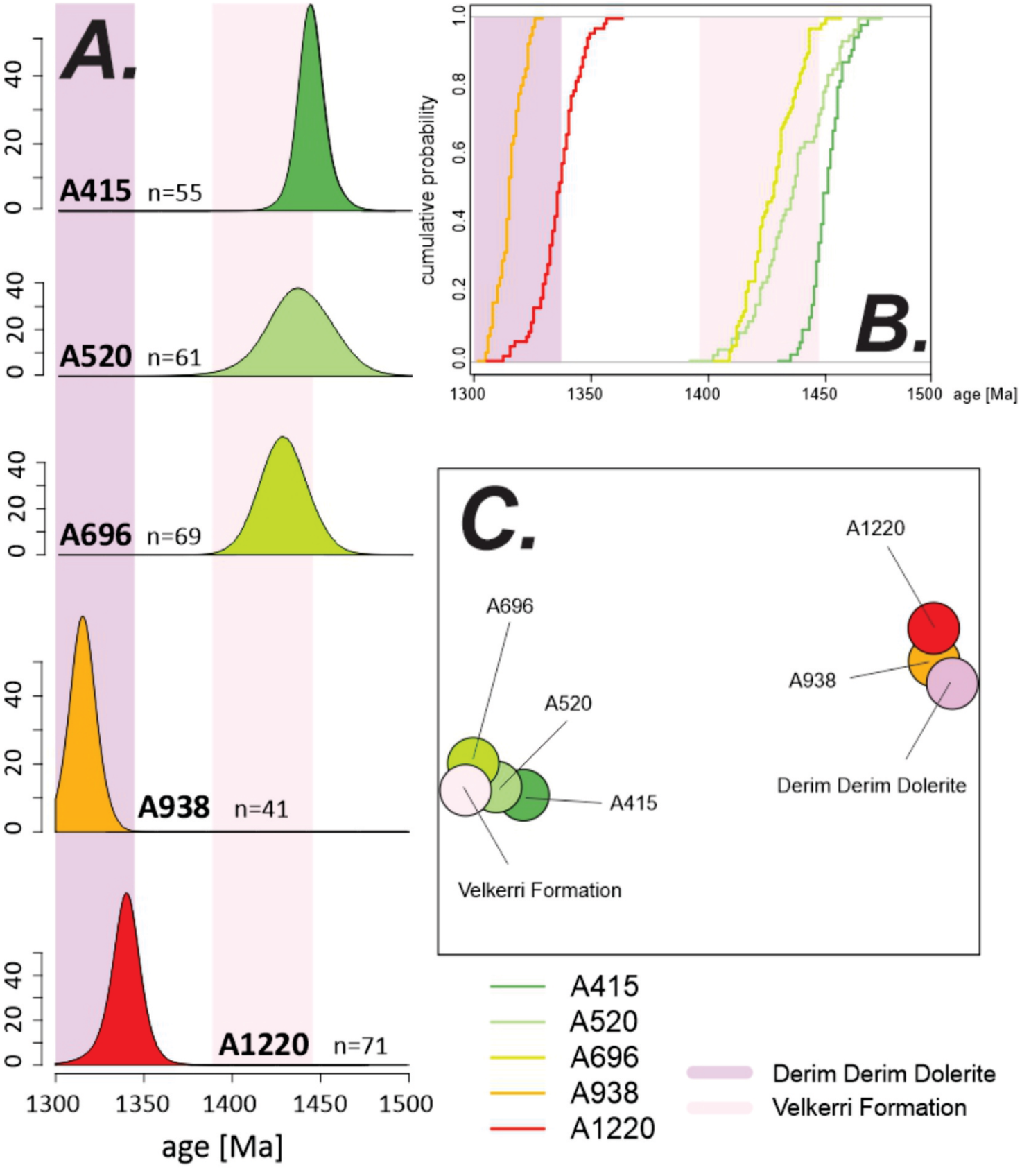
A.
A415 n=55
A520 n=61
A696 n=69
A938 n=41
A1220 n=71
0 20 40
1300 1350 1400 1450 1500
age [Ma]
B.
cumulative probability
0.0 0.2 0.4 0.6 0.8 1.0
1300 1350 1400 1450 1500 age [Ma]
C.
A1220
A696
A938
A520
A415
Derim Derim Dolerite
Velkerri Formation
A415
A520
A696
A938
A1220
Derim Derim Dolerite
Velkerri Formation

Figure 9

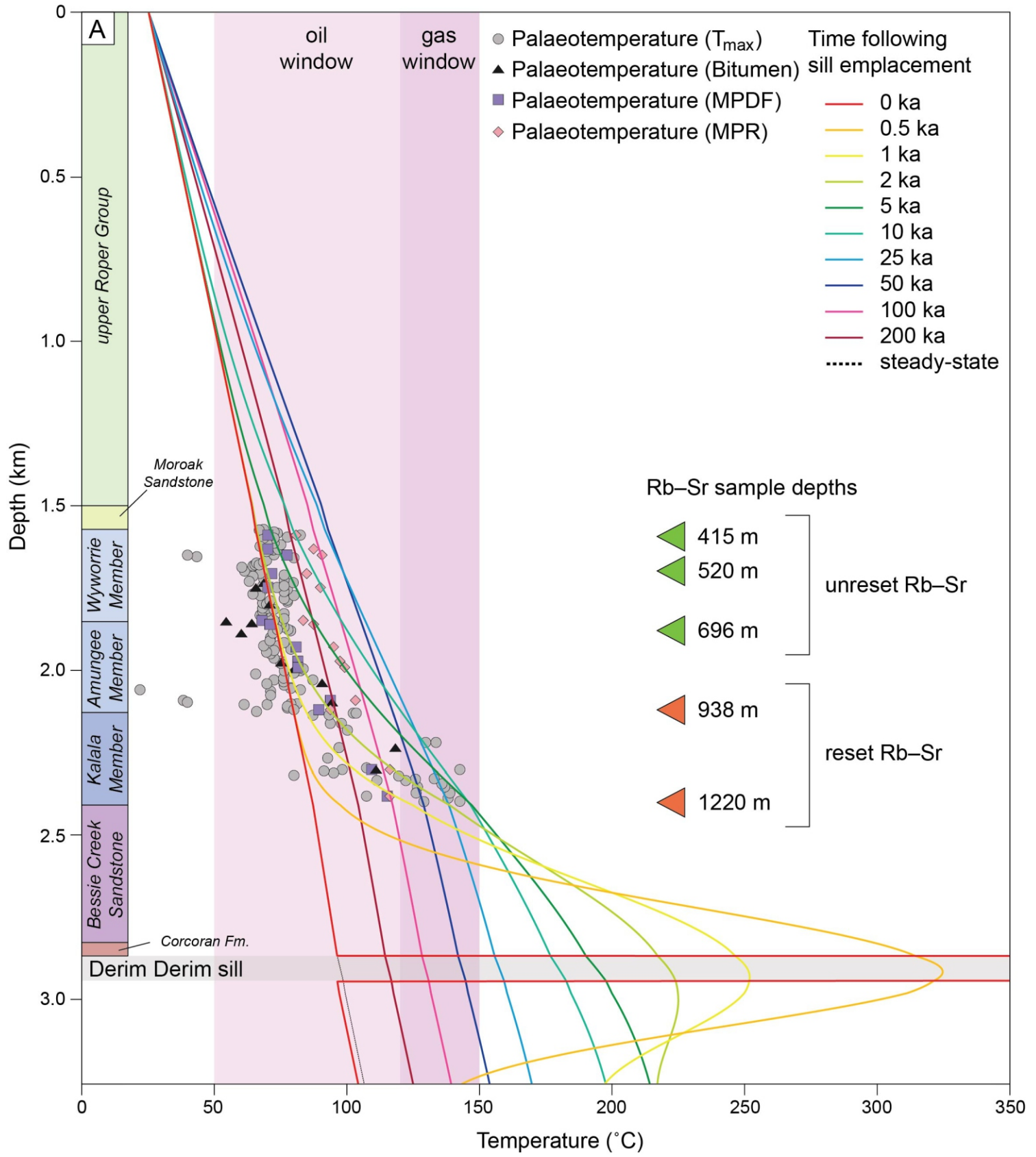
A
oil window
gas window
Palaeotemperature (T_{max})
Palaeotemperature (Bitumen)
Palaeotemperature (MPDF)
Palaeotemperature (MPR)
Time following sill emplacement
0 ka
0.5 ka
1 ka
2 ka
5 ka
10 ka
25 ka
50 ka
100 ka
200 ka
steady-state
Rb–Sr sample depths
415 m
520 m
696 m
938 m
1220 m
unreset Rb–Sr
reset Rb–Sr
upper Roper Group
Moroak Sandstone
Wyworrie Member
Amungee Member
Kalala Member
Bessie Creek Sandstone
Corcoran Fm.
Derim Derim sill
Depth (km)
Temperature (˚C)

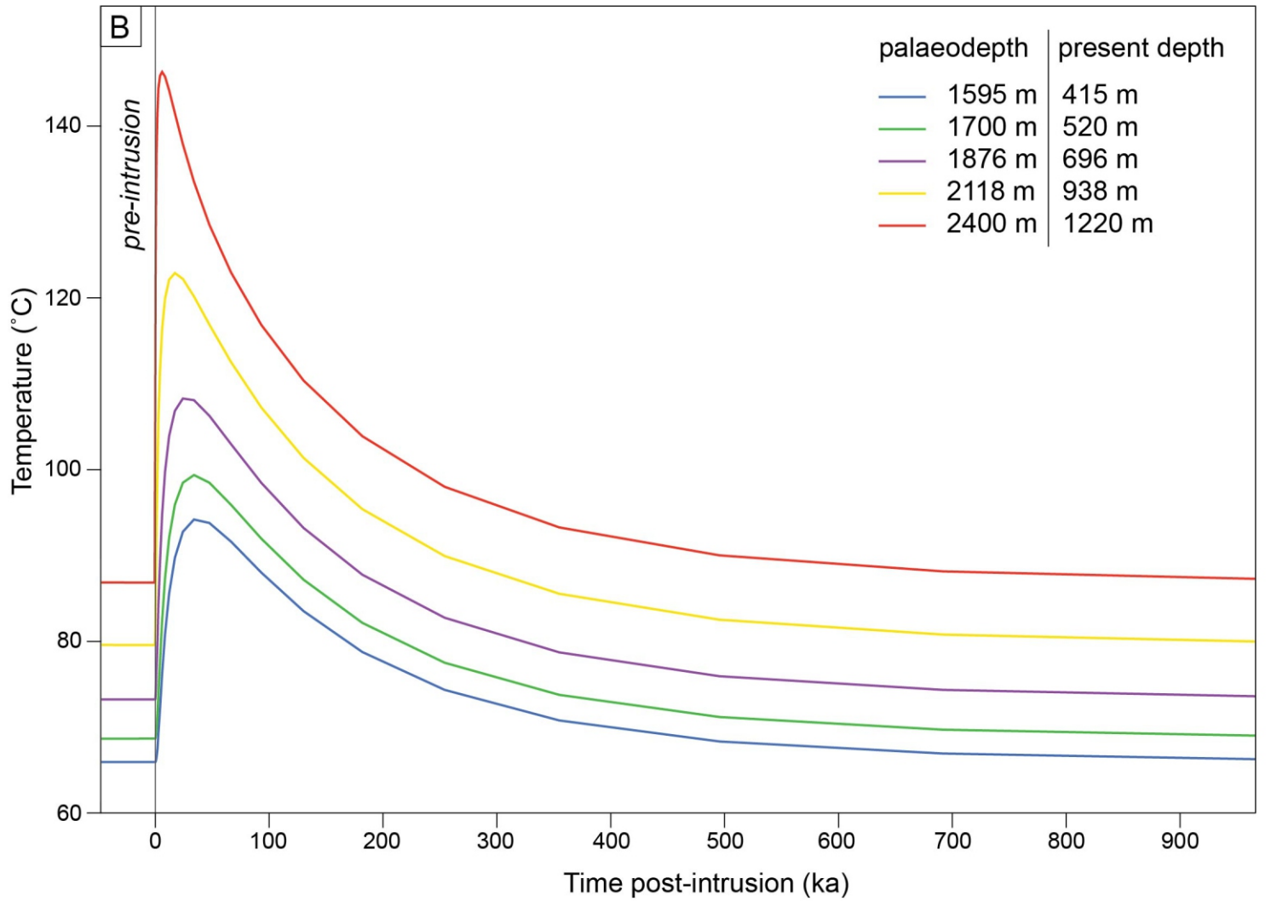
B
pre-intrusion
palaeodepth
present depth
1595 m
415 m
1700 m
520 m
1876 m
696 m
2118 m
938 m
2400 m
1220 m
Temperature (˚C)
Time post-intrusion (ka)